

Cardiac gene delivery using ultrasound: State of the field

Davindra Singh,¹ Elahe Memari,² Stephanie He,¹ Hossein Yusefi,² and Brandon Helfield^{1,2}

¹Department of Biology, Concordia University, Montreal, QC, Canada; ²Department of Physics, Concordia University, Montreal, QC, Canada

Over the past two decades, there has been tremendous and exciting progress toward extending the use of medical ultrasound beyond a traditional imaging tool. Ultrasound contrast agents, typically used for improved visualization of blood flow, have been explored as novel non-viral gene delivery vectors for cardiovascular therapy. Given this adaptation to ultrasound contrast-enhancing agents, this presents as an image-guided and site-specific gene delivery technique with potential for multi-gene and repeatable delivery protocols—overcoming some of the limitations of alternative gene therapy approaches. In this review, we provide an overview of the studies to date that employ this technique toward cardiac gene therapy using cardiovascular disease animal models and summarize their key findings.

INTRODUCTION

Ultrasound is one of the most widely used imaging modalities to assess and diagnose conditions of the heart, in part due to its real-time, non-ionizing nature. Ultrasound contrast agents, which consist of a suspension of small encapsulated bubbles between 1 and 5 μm in diameter, are strong reflectors of ultrasound and enhance the signal from the blood pool to which they are confined, adding diagnostic utility in the assessment of blood flow and perfusion.¹ Leveraging the excellent safety profile of medical ultrasound and the near global approval of microbubble contrast agents, recent work has explored the possibility of extending its use toward image-guided therapy for a range of disease conditions.² Perhaps one of the most notable approaches is using these microbubbles for the purpose of targeted nucleic acid therapeutics. Either through co-injection or via attachment of a genetic payload, ultrasound-triggered microbubbles can be made to locally deposit molecular therapeutics within a target diseased tissue. Currently, the most clinically advanced application of this technique is brain therapy via the reversible opening of the blood-brain-barrier under magnetic resonance imaging (MRI) guidance (e.g., Alzheimer's disease³).

Cardiovascular disease (CVD), however, has long been envisioned as a candidate for such a gene therapy, which, despite advancements in pharmacological and imaging approaches, remains a major cause of morbidity and mortality in North America and worldwide.⁴ Despite initial trials showing neutral or modest results, significant advancements in the development of gene delivery vehicles, specifically non-viral techniques, have brought it back into the spotlight.^{5,6} As

such, ultrasound-mediated gene delivery within the context of CVD holds tremendous promise since this approach⁷ is (1) non-viral, which avoids potential immunogenic responses and dose-limiting side effects; (2) can be inherently image-guided, as these bubbles still function as ultrasound-enhancing agents; (3) non-invasive, which opens the opportunity for protracted, repeated therapy; and (4) integrates nicely within the clinical arena, as echocardiography is a common approach toward the initial diagnosis of many CVDs. In fact, this technique has been shown feasible for the delivery of many types of molecular therapeutics (Table 1).

In this review, we provide an overview of ultrasound-mediated gene delivery to the heart. We acknowledge that this a subset of the applications for which microbubble-mediated therapies have been demonstrated, both within CVD (e.g., vascular disease⁸) and outside of it (e.g., cancer,⁹ blood-brain-barrier-based approaches³). We do touch upon some of these topics but refer the reader to excellent, recent reviews on those subject matters.¹⁰ Here, we begin with setting the context for this review by a brief survey of current gene therapy approaches for CVD, followed by an overview of microbubble dynamics within an ultrasound field to provide context for their use in targeted CVD gene therapy; and continue with a summary of postulated microbubble-based bioeffects and bubble agents that are employed for ultrasound-assisted gene therapy. Next, we provide an overview of the preclinical *in vivo* studies to date that specifically target the heart. Finally, we provide an outlook on this exciting inherently image-guided approach to targeted cardiac gene delivery.

CURRENT METHODS FOR CARDIAC GENE DELIVERY

Perhaps the most direct and earliest approach is the naked delivery of molecular therapeutics via surgical intervention.^{11,12} Recently, the clinical study EPICCURE (NCT03370887) was the first to report direct epicardial injection of naked mRNA encoding vascular endothelial growth factor (VEGF)-A.¹³ This trial demonstrated an excellent safety profile with no severe adverse affects, yet the relatively small sample size rendered interpretation of the efficiency challenging. While very promising, naked delivery is typically characterized with sub-optimal gene uptake,¹⁴ and direct needle injection into

<https://doi.org/10.1016/j.omtm.2024.101277>.

Correspondence: Brandon Helfield, Departments of Physics and Biology, Concordia University, 7141 Sherbrooke Street W., Montreal, QC H4B 1R6, Canada.
E-mail: brandon.helfield@concordia.ca



Table 1. Summary of vectors, along with select examples, that have been used in conjunction with ultrasound for targeted delivery in the context of CVD

Vector	Example gene
Plasmids	VEGF, ⁸ S100A6, ⁸⁹ Ang1 ¹¹⁸
siRNAs	ICAM-1, ¹¹⁹ galectin-7 ¹²⁰
miR	miR-21, ¹²¹ miR-126 ¹⁰⁹
Anti-miR	antimiR-23a, ⁶³ antimiR-155 ¹²²
Piggybac	GLP-1, ¹²³ ANGPTL8 ¹²⁴
Minicircle DNA	VEGF ¹⁰⁶

Ang1, angiopoietin-1; ANGPTL8, angiopoietin like protein 8; GLP-1, glucagon-like peptide; ICAM-1, intercellular adhesion molecule-1; miR, microRNA; S100A6, S100 calcium binding protein A6; VEGF, vascular endothelial growth factor.

the target poses challenges in achieving homogeneous tissue distribution, potential localized damage from the needle, and clinical implementation is limited by the impracticality of repetitive needle injections into sites that may be difficult to access.^{15,16}

The most recognized vehicle-based method of cardiac gene therapy to date is the use of viral vectors. Robust preclinical research has revealed two viral vector systems that yield effective gene transfer: adenovirus and adeno-associated virus (AAV).⁶ Earlier works with adenovirus vectors have advanced to clinical trials for heart failure¹⁷; however, this type of vector still retains many adenoviral genes and results in strong inflammatory cascades that raise safety concerns. The gold-standard viral approach is the use of AAVs,¹⁸ which despite their proven efficiency, are still met with limitations including packaging capacity, tissue specificity, and immune evasion—all areas of active research.¹⁶ Additionally, unlike adenovirus methods in which transgene expression returns to baseline over the time course of a few weeks,¹⁹ AAV methods result in permanent transgene expression. While this presents safety concerns in terms of off-target effects, it may also not be desirable from a pathophysiology viewpoint.²⁰ The strategy for delivery for these viral vectors remains relatively invasive, with one of the more common approaches the direct intramyocardial injection either through surgical access or through intraventricular delivery via percutaneous catheter.

Attempts to address these concerns have led to more recent work exploring the use of non-viral approaches, one example of which is lipid nanoparticles (LNPs) as a delivery vehicle. Indeed, LNP formulations of small molecule drugs represent a relatively mature technology,²¹ and considerable research is ongoing to expand their application to gene delivery.²² The first such application of LNP-mediated gene delivery with significant *in vivo* efficiency was demonstrated in 2006, carrying small interfering RNA (siRNA) to silence genes in hepatocytes.²³ While there is much investigation into the lipid composition and overall design of gene-bearing LNPs, this approach is still limited in the context of CVD; including the resulting immune response to LNP formulations of RNA and DNA, and challenged by delivery to non-hepatocyte tissues, in part due to a lack of mech-

anistic understanding of their systemic biodistribution.²⁴ Beyond LNPs, extracellular vesicles (EVs), which are cell-derived lipid nanoparticles typically involved in cell-to-cell communication, have gained a lot of traction in recent years as non-viral gene delivery vectors.²⁵ Intrinsic benefits of EVs include their stability, increased propensity for cellular uptake, and their ability to avoid interaction with the immune system.²⁶ Recent studies have demonstrated the potential for EV-based gene therapy for CVD,^{27–30} and while such studies highlight the exciting promise of this methodology, several challenges need to be addressed, including the development of techniques for the characterization of EV cargo, design and integration of platforms to monitor the vesicles *in vivo*, and the development of strategies to modify EVs to improve their targeted accumulation in specific tissues.³¹ To this end, recent work has demonstrated improved cardiac retention of intramyocardial delivered EVs by using genetic modifications to incorporate cardiac binding peptides on their surface.³²

Either alone or in combination with the current and emerging approaches listed here, ultrasound-assisted cardiac gene delivery using contrast agent microbubbles has many advantages, including its non-viral nature, the inherent image guidance, and excellent gene localization potential.

BRIEF OVERVIEW OF THE SALIENT FEATURES OF MICROBUBBLES

Owing to the compressibility of the gas core, microbubbles vibrate as they pass through the acoustic beam, expanding and contracting about their resting, equilibrium radius R_0 . Microbubble agents are polydisperse and exhibit resonance; the specific frequency at which a given bubble vibrates with maximum amplitude is inversely related to its size.³³ Microbubble vibrations can be broadly subdivided into two categories (Figure 1). Under low acoustic intensity, microbubbles undergo periodic oscillations about their equilibrium size resulting in echoes that possess a rich resonant structure, exhibiting energy at harmonic frequencies (integer multiples of the transmit frequency) and often sub-harmonic frequencies (half-order multiples of the transmit frequency).³⁴ This type of vibration is often termed stable oscillation, which is desired in routine contrast imaging. In this vibration regime, microbubbles generate local shear forces on neighboring cells and tissue, as well as local fluid streaming (termed microstreaming).³⁵ Under higher intensities, microbubbles can be made to disrupt due to rapid expansion and subsequent violent bubble collapse. This vibration regime, termed inertial cavitation, can generate highly localized increases in pressure and temperature, which may result in shock wave production or the formation of high-speed liquid jets.³⁶ The propensity for microbubbles to initiate sustained stable cavitation or inertial cavitation is defined by a confluence of factors, not the least of which is the mechanical index (MI), defined as the acoustic pressure scaled by the square root of the frequency.³⁷

OVERVIEW OF ULTRASOUND-ASSISTED GENE DELIVERY

It was first observed in the late 1990s that ultrasound-mediated microbubble activity can result in vessel permeability.^{38,39} These

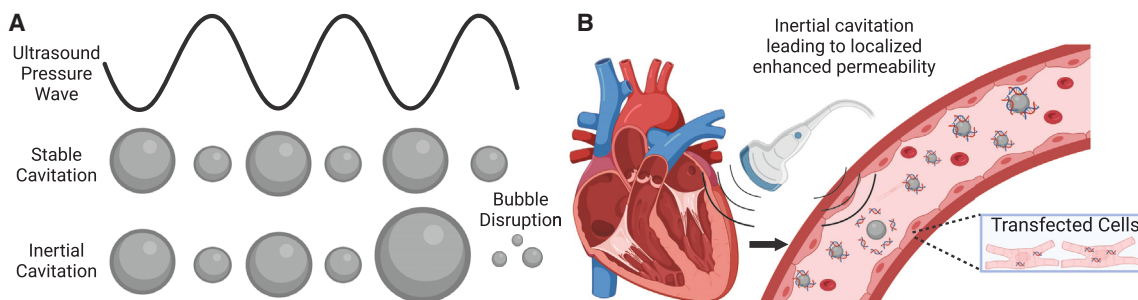


Figure 1. Schematic diagram depicting the concept of stable versus inertial cavitation and cardiac gene delivery

(A) Stable cavitation consists of periodic vibrations, whereby the bubble gets bigger during rarefaction and smaller during the compressional phase. Inertial cavitation is the process whereby large bubble expansion results in subsequent bubble disruption. (B) Externally applied ultrasound to the heart can result in local bubble cavitation and/or molecular therapeutic release. Enhanced cellular and vascular permeability results in transfection of target cells. Note that two main strategies exist: co-injection of standard microbubbles with a molecular therapeutic, and gene-bearing microbubbles (shown here).

studies spurred the onset of many mechanistic physical and biological investigations, as well as application-driven research aimed at harnessing this bioeffect for therapeutic purposes. With respect to gene delivery, the concept is to promote such transient cellular and vascular permeability while simultaneously depositing a nucleic acid payload to the target tissue of interest. As microbubbles remain intravascular, successful gene delivery to the heart first requires interaction between them and endothelial cells. In this section, we briefly describe microbubble-induced endothelial permeabilization and outline some of the approaches toward ultrasound gene delivery.

Microbubble-mediated bioeffects on endothelial cells

In one of the earliest mechanistic, real-time studies conducted in the context of microbubble-endothelial cell interactions,⁴⁰ it was observed that vibrating bubbles in contact with an endothelial cell result in plasma membrane deformation due to the local fluid motion (i.e., a pushing and pulling effect). It was later determined that bubble vibration amplitude, itself a function of intensity and other intrinsic factors, is a threshold indicator for localized, resealable endothelial membrane perforation and the loosening of intercellular junctions⁴¹ (Figure 2). The shear stress induced by the vibrating microbubbles on the neighboring endothelial cells triggers calcium ion influx^{42–44} and local ATP release,⁴⁵ which is responsible for many downstream cellular and vascular processes including flow augmentation and vasoactivity.⁴⁶ Even without direct endothelial cell permeability, the mechanical stress generated by microbubble oscillations has been shown to stretch the blood vessel wall,⁴⁷ activate mechanosensitive ion channels, and open up otherwise tight intra-endothelial junctional contact^{48,49} providing a paracellular entry route for gene delivery. Indeed, given the enhanced local permeability of the vasculature, one of the advantages of this approach is that it does not in principle require activation of endocytic pathways and thus payloads do not require release from early endosomes to be effective. However, there is mounting evidence that locally vibrating microbubbles do have an influence on endothelial endocytosis,^{50,51} which may play either a primary or an ancillary role in transcellular delivery routes.

There are many investigations confirming microbubble-mediated transient vascular permeability enhancement without evidence of vascular rupture.⁵² These studies, broadly speaking, are conducted using pulsed ultrasound (~ 0.1 – 10 ms) and low duty cycles, resulting in restoration of native endothelial permeability on the order of 1–2 min,⁵³ and vascular barrier function from minutes to hours,⁵⁴ depending on the pulsing scheme and tissue type. However, it is important to note that large-magnitude microbubble vibration may cause local damage to neighboring endothelial cells and tissue. Excessive driving force (e.g., MI, burst length, duty cycle, exposure duration) will result, all else equal, in large microbubble excursions and increased probability of violent bubble collapse.³⁴ Prolonged perforation, whether it be due to very large perforations or those that do not reseal in a timely manner, have been shown to cause endothelial cell death.^{44,55} Indeed, aside from bubble vibration characteristics, there is a limited set of experimental data that highlights that perforation time course is also a function of biological regulatory mechanisms (e.g., availability of calcium ions,⁵⁶ plasma membrane constituents⁴⁴). On the vascular level, treatment with exceedingly large MI (~ 1.3 – 2.0) under certain acoustic schemes can cause vascular rupture and hemorrhage,^{57–59} although the specific damage thresholds will depend on a range of acoustic (e.g., pulse scheme, microbubble composition and concentration) and non-acoustic (e.g., vessel properties, tissue type) variables.^{60,61}

Microbubble gene carrier agents

With respect to the delivery approach, there are two main strategies. The first is via a co-injection of both microbubble agent and the molecular therapeutic. While this can be done with in-house synthesized agents, the microbubbles used here are similar to those commonly clinically used in medical imaging. In fact, clinical agent Definity, Optison, and SonoVue have all been used for this purpose. Combining a Food and Drug Administration (FDA)/Health Canada approved microbubble agent and an approved molecular therapeutic is likely advantageous for easier entry into clinical trials.

The second strategy is through the design of newly constructed gene-bearing agents. While many design types exist (see Lentacker

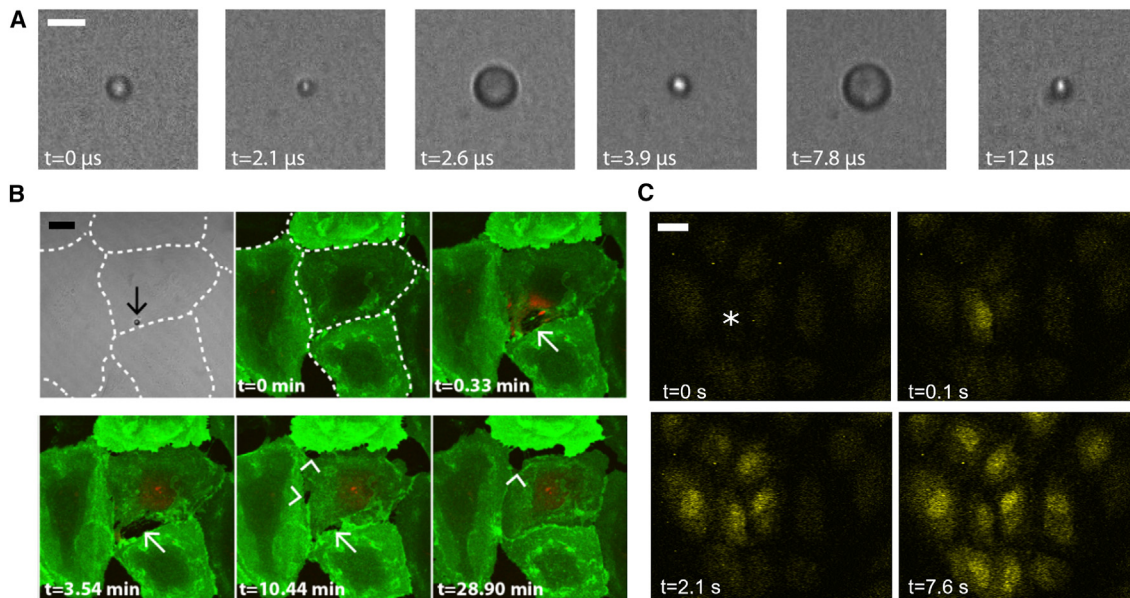


Figure 2. Ultrasound-enhancing agents vibrate in the vasculature and can give rise to local and reversible increases in vascular permeability and modulate intercellular signaling

(A) Ultrafast-frame camera recording of a single gas-filled microbubble contrast agent oscillating under 1 MHz ultrasound ($MI = 0.8$). This vibration generates local shear stress on neighboring tissue. Scale bar, 5 μm . (B) An individual microbubble (black arrow) can reversibly perforate endothelial cell plasma membrane (green) to locally deliver a therapeutic (red). White-dotted lines demarcated each endothelial cell. The white arrow depicts the resealable perforation caused by the single microbubble and the white arrowheads denote intercellular gaps between adjacent endothelial cells. $MI = 0.8$. Scale bar, 25 μm . Modified from Helfield et al. PNAS 2016⁴¹ with permission. (C) Individual microbubble oscillation (white asterisk) causes a direct increase in intracellular Ca^{2+} (yellow) as well as intercellular Ca^{2+} signaling to neighboring, non-treated cells. Scale bar, 25 μm . Modified from Helfield et al. Ultrasound Med Biol. 2020⁴⁴ with permission.

et al.⁶² for a nice overview), the most common approach used in preclinical cardiac delivery work is through the development of a cationic lipid-encapsulated agent, whereby nucleic acid payloads are charge-coupled to the surface of the bubbles.^{8,63} In principle, this ensures that the microbubble activity and local nucleic acid concentration are spatially temporally coherent, that is to say that the presence of the molecular therapeutic remains in close proximity to the ultrasound-induced permeability-enhancing effect, and that it protects the nucleic acid payload from degradation. However, this brings along new considerations as to whether the same ultrasound conditions that “shake” off the drug from the bubble (which will be a function of how strongly bound the polyanion is to the cationic lipid) are the same conditions that result in safe, repeatable vascular and cellular permeability. Additionally, incorporation of the therapeutic within the bubble design can also limit the payload size.

Non-cardiac implementation of ultrasound-assisted gene delivery

Currently, the most advanced application of ultrasound-assisted gene therapy is within the context of delivery to the central nervous system (CNS).⁶⁴ Over the past 12 years, MRI-guided focused ultrasound has demonstrated successful gene delivery in preclinical models (e.g., mice, rats, non-human primates).⁶⁵ This progress is largely owed to the expansive research spanning decades into the localized and

reversible opening of the blood-brain-barrier via focused ultrasound.^{66–70} Indeed, MRI-guided microbubble-mediated opening of the blood-brain-barrier is a rapidly expanding technology currently in clinical trials within the context of oncology (e.g., NCT03626896), Alzheimer’s (e.g., NCT03739905), and Parkinson’s disease (NCT03608553). In neuro-oncology patients, which is the most clinically advanced sub-area, promising pilot clinical studies have confirmed feasibility of this technique for the targeted delivery of chemotherapeutics (e.g., temozolomide,⁷¹ carboplatin⁷²) and immunotherapies (e.g., monoclonal antibodies^{73,74}). Simultaneously to this, there is active research on utilizing the acoustic feedback of the microbubble vibrations to control the acoustic beam in order to localize the intended bioeffects and minimize unintended damage.^{75–77} These treatments are performed with specifically designed transducer systems, either transcranial (e.g., ExAblate Neuro; Insightec, Haifa, Israel) or implanted (e.g., SonoCloud, CarThera, Paris, France), to achieve the desired treatment and/or acoustic monitoring function.⁷⁸

Aside from this, there is ongoing preclinical research on ultrasound-assisted gene therapy to extracranial applications, which for the most part utilize single-element or commercial array transducers, including ocular disease,⁷⁹ cancer,^{9,80} and diabetes.⁸¹ A subset of this work employs separate, co-aligned transducers to provide some indication of microbubble activity throughout the treatment.

Table 2. Pillars of gene therapy targets for CVD

Gene therapy pathway targets for CVD	Example genes
1. Promoting angiogenesis	VEGF-165, ¹²⁵ FGF-4 ¹²⁶
2. Modifying CM Contractility	SERCA2a, ¹²⁷ AC6 ¹²⁸
3. Apoptosis inhibition	AM, ¹²⁹ Bcl-2 ¹³⁰
4. Superseding cell checkpoints to promote CM proliferation	Wnt11 ¹³¹
5. Increasing cytoprotective mechanisms	VEGF-B167, ¹³² HO-1 ¹³³
6. Exogenous cardiac stem cells or progenitors	SDF-1 ^{134,135}

AC6, adenyl cyclase 6; AM, adrenomedullin; Bcl-2, B-cell lymphoma 2; CM, cardiomyocyte; CVD, cardiovascular disease; FGF-4, fibroblast growth factor 4; HO-1, heme oxygenase-1; SDF-1, stromal-cell-derived factor 1; SERCA2a, sarcoplasmic/endoplasmic reticulum Ca²⁺ ATPase.

APPLICATIONS OF ULTRASOUND-ASSISTED GENE DELIVERY TO THE HEART

Recent advances in identifying key molecular pathways and genes involved in the initiation and evolution of CVD have enabled the concept of targeted molecular therapeutics. The genes that are selected as a target molecular therapeutic for CVD broadly fall into several categories,⁵ summarized in Table 2. There is a wide array of preclinical studies in animal models investigating CVD gene therapy, using a wide range of target genes highlighting successful and promising results. This has led to several clinical trials examining this technology toward translation to human patients, but despite their careful design, many of these trials show either neutral or modest benefit.⁸² This highlights the need to examine the details of these approaches, from the initial gene selection, vector dosing, frequency of administration, and the mode of delivery—all in relation to the target disease process and its stage. When considering the mode of delivery, the typically employed method of choice is viral vectors. Although currently available vectors have demonstrated promising transduction to cardiac tissue, undesired side effects, including non-specific uptake in non-target tissue and the presence of neutralizing antibodies against the gene products may be limitations moving forward.⁵

In recent years, ultrasound-assisted gene therapy has been gaining traction as a non-invasive, non-viral tool to tackle some of the limitations described above. The “controllability” of this approach, granted by spatial targeting of the ultrasound beam, along with its inherent image-guided nature, make it an attractive option for cardiac gene delivery. The first application of this approach was demonstrated over 2 decades ago, in which healthy rodents were subjected to ultrasound in conjunction with albumin microbubbles linked to β -galactosidase and exhibited a myocardial expression over 10-fold more than untreated controls 4 days post treatment.⁸³ As an exhaustive summary of all ultrasound-assisted CVD gene therapies is out of the purview of this review, the following sections summarize applications in which ultrasound-assisted gene therapy targeted toward the heart (as opposed to peripheral tissue⁸) has been demonstrated in diseased animal models (as opposed to pure proof-of-principle studies in healthy models⁸⁴); the summary of which is presented in Table 3.

Myocardial infarction

Acute myocardial infarction is one of the more severe manifestations of coronary heart disease, which is attributed to over 40% of all deaths due to CVD in the United States.⁴ Perhaps one of the first applications of functional gene delivery to the heart in an acute myocardial infarction model was demonstrated by Kondo and colleagues⁸⁵ via the delivery of hepatocyte growth factor (HGF) in a rat model. HGF plays a role in preventing myocyte death due to oxidative stress and cardiomyocyte apoptosis during reperfusion. In fact, it has been demonstrated through viral approaches that gene delivery of HGF before myocardial infarction attenuates reperfusion injury and induces angiogenesis in infarcted myocardium.⁸⁶ Starting 2 h after coronary ligation, plasmid HGF (1.5 mg) was infused into the left ventricle (LV) via catheter for 1.5 min while simultaneous clinical contrast agent Optison was injected in the femoral vein at 0.2 mL/min for 5 min.⁸⁵ In the treatment groups, echocardiography was administered using a Philips Sonos 5500 system (S3 probe) operating in ultraharmonic mode at 1.3 MHz and an MI = 1.8 for 4 min, triggered every eighth end-systole. A week post surgery, HGF was quantified using immunohistochemistry, revealing homogeneous expression in the treated groups compared with patchy or non-existent expression in HGF alone and negative control groups respectively. At 3 weeks post treatment, serial echocardiography measurements confirmed that LV mass was decreased, and histology data revealed reduced scar size, and capillary/arterial density was much improved in the treated groups compared with controls.

More recently, studies are beginning to explore the synergistic effects of gene therapy in conjunction with stem cell therapies. Wang and colleagues⁸⁷ demonstrated the simultaneous delivery of two genes: SERCA2a, which regulates cardiac contraction and relaxation by controlling intracellular Ca²⁺ handling, and Cx43, well-known to mediate electrical coupling between cardiomyocytes via gap junctional intracellular communication. Dual-gene therapy was performed in a rat model of acute myocardial infarction both with and without pretransplantation of bone mesenchymal stem cells (BMSCs) 4 weeks post ligation surgery. Their motivation here was the hypothesis that BMSC transplantation would amplify the effect of gene transfection by providing better preconditioning in the border zone. Four weeks after treatment, they observed about a factor of 2x increase in SERCA2a and Cx43 protein expression relative to non-treated controls in both the infarct and border zones, with no difference in remote cardiac tissue and no change in infarct size. Further, echo measurements confirm greater LV ejection fraction (LVEF) and LV fractional shortening (LVFS) compared with control groups, and that LV function was improved slightly in treated model rats that were pre-conditioned with BMSCs (~4%–5% increase in LVEF and LVFS).

Ischemia/reperfusion injury

Early work by Erikson and colleagues⁸⁸ investigated the use of anti-sense oligodeoxynucleotides (ODNs) as a gene therapy strategy to attenuate expression of tumor necrosis factor (TNF)- α in a rat model of ischemia/reperfusion (I/R) injury. Using a 1-MHz treatment

Table 3. Summary of ultrasound-assisted gene delivery to the heart in preclinical CVD models

Author	GOI/Model/Targeted pathway ^a /Injection route	Ultrasound settings	Results summary
Ischemic heart disease			
Wang et al. 2022 ⁸⁷	Cx43 and SERCA2a/Rat/#2/tail vein (intravenous [i.v.])	US system: Kunlun 7 (Mindray) Probe/Frequency: L11-3 U Pressure/Power: MI = 1.0 Pulse length: Single flash frame Interval: Triggered manually every 3–5 s Total duration: 10 min. MB: Single treatment with in-house gene-carrying lipid agent (@4 × 10 ⁹ MB/mL); injection volume of 100 μL consisting of bubble-bound to Ad-encoding of either Cx43, SERCA2a or both (MOI of 500); infused via tail vein at 15 mL/h.	Direct readout: About a 2-fold increase in protein levels of SERCA2a and Cx43 using dual-gene-carrying microbubbles at 4 weeks post treatment in the infarct zone; similar result for each protein using the single-gene-loaded bubble. Other details: BMSCs were transplanted by myocardial injection 4 weeks post ligation surgery. Modest improvements in LVEF and LVFS in treated groups with BMSC pre-treatment, but no change in infarct size.
Cao et al. 2021 ¹¹⁸	Ang1/Canine/#1/elbow vein (i.v.)	US system: Single element Probe/Frequency: 0.3 MHz Pressure/Power: 2W/cm ² Pulse length: 10s Interval: PRI of 10s Total duration: 20 min. MB: Single treatment 24 h post surgery with co-loaded SonoVue and Ang1 plasmid (0.25 mg/mL) cocktail resulting in 1.5 × 10 ⁸ MB/mL; a 2-mL volume was infused at 12 mL/h.	Direct readout: At 30 days post surgery, they showed a 3x increase in Ang1 compared with a negative control plasmid delivery. Other details: Compared with untreated controls, they observed an increase in microvascular density, decrease in sympathetic nerve density, and increase in LVEF and LVFS.
Sun et al. 2020 ¹³⁶	SDF-1/Rat/#6/caudal vein (i.v.)	US system: Single element Probe/Frequency: 1 MHz Pressure/Power: 2W/cm ² Pulse length: DC of 50% Interval: PRF of 1 kHz Total duration: 2 min MB: One to three treatments (in 2-day intervals) of in-house lipid agent (4 × 10 ⁹ MB/mL) in a 0.5-mL volume with 250 μg of plasmid DNA infused at 15 mL/h. Post-treatment, infusion of shRNA-PHD2 modified BMSCs (1 mL).	Direct readout: Compared with controls, authors also observed an ~2x increase in SDF-1 after a single US + MB treatment. Other details: Main results are increased BMSC survival, reduced myocardial apoptosis, reduced infarct size, increased vascular density, and improved cardiac function (LVEF and LVFS at 4 weeks post) compared with the controls following a three- treatment regimen.
Zhang et al. 2017 ¹³⁷	shRNA for PHD2/Rat/#1/tail vein (i.v.)	US system: Sonitron 2000V (Nepa Gene) Probe/Frequency: 1 MHz Pressure/Power: 2W/cm ² Pulse length: Not specified. Interval: DC of 50% Total duration: 2 min. MB: Three treatments with in-house gene-carrying lipid bubble (~4 × 10 ⁹ MB/mL) containing 600 μg/kg of shRNA 0.5-mL sample was infused at 15 mL/h.	Direct readout: At 4 days post treatment, they observed a 57% decrease in PHD2 mRNA levels and a 39% decrease in PHD2 protein levels compared with untreated controls. Other details: Treatments on day 0 (10 min after ligation), day 2, and day 4 with cationic microbubbles. LVFS and LVEF significantly increased at 4 weeks.
Deng et al. 2015 ¹³⁸	Ang1/Rabbit/#1/ear vein (i.v.)	US system: iE33 (Philips) Probe/Frequency: M3S/1.7 MHz Pressure/Power: MI of 1.3 Pulse length: Single flash frame Interval: Triggered every 4–8 cardiac cycles Total duration: 5 min. MB: Single treatment. Co-injection of either SonoVue or ICAM-1 decorated SonoVue	Direct readout: Compared with single treatment with standard SonoVue, the targeted MB treatment resulted in approximately 1.7x increase in Ang-1 mRNA and 1.2x increase in Ang-1 protein expression. Pure negative controls expressed no human Ang-1. Other details: Compared with controls, a 1.6x increase in microvessel density, and LVEF, LVIDd, and LVAWd all increased at 2 weeks.

(Continued on next page)

Table 3. Continued

Author	GOI/Model/Targeted pathway ^a /Injection route	Ultrasound settings	Results summary
		and 100 µg of plasmid in a 1-mL volume. Details on infusion speed/time were not provided.	
Liu et al. 2015 ¹³⁹	miR-21/Porcine/#5/ear vein and LAD	US system: Not specified. Probe/Frequency: 1 MHz Pressure/Power: 1–3 W/cm ² Pulse length: Not specified. Interval: DC of 50% Total duration: 20 min. MB: Single treatment with in-house lipid bubble; co-injection with miR-21 (4 mg) in a volume of 6 mL (~1.9 × 10 ⁹ MB/mL). Details on infusion speed/time were not provided.	Direct readout: Approximately 12–15x higher levels of miR-21 after 4 days in the heart, with the higher delivery efficiency observed via intracoronary injection vs. i.v. Other details: The authors assayed for PDCD4 protein expression, a downstream target of miR-21, and showed a significant decrease of PDCD4 (~40% decrease) compared with control.
Li et al. 2015 ¹⁴⁰	MSCs/Rat/#6/caudal vein (i.v.)	US system: Acuson S2000 (Siemens) Probe/Frequency: 2 MHz Pressure/Power: MI = 1.3. Pulse length: Not specified. Interval: Not specified. Total duration: 10 min. MB: Single treatment. In-house lipid bubble (0.1 mL/kg @ 7.5 × 10 ⁹ MB/mL) co-injection with MSCs. Details on infusion speed/time were not provided.	Direct readout: Results show increase in the number of homing MSCs (1.3x increase) in the US-treated group compared with non-treated controls. Other details: Higher protein expression of SDF-1 (1.9x) and CXCR4 (~1.5x) were observed in the ischemic myocardium treated vs. control groups.
Sun et al. 2013 ⁹³	AKT/Rat/#1/tail vein (intravenous)	US system: Vivid 7 (GE) Probe/Frequency: M3S/1.6 MHz Pressure/Power: MI = 1.3 Pulse length: Single flash frame Interval: ECG triggered every fourth end-systole Total duration: 20 min. MB: Single treatment with in-house gene-carrying lipid bubble or Definity containing 0.2 mg/kg of plasmid DNA. 0.4-mL sample was infused at 1.2 mL/h.	Direct readout: Three days post treatment, protein levels of AKT were increased using either Definity (1.3x) or the in-house agent (1.7x) compared with untreated control. Other details: Other protein targets included p-AKT (~1.7x for Definity; 2.5x for in-house), survivin (1.1x for Definity; 1.3x for in-house) and p-BAD (2x for Definity; 3x for in-house). Treatment with the in-house agent lowered infarct size, increased infarct thickness, reduced apoptosis, increased vascular density (after 3 days), and improved cardiac function/perfusion (21 days) compared with using Definity and to non-treated controls.
Zhou et al. 2013 ¹⁴¹	HGF/Rat/#1/femoral vein (i.v.)	US system: CGZZ ultrasonic gene transfection instrument Probe/Frequency: 0.3 MHz Pressure/Power: 2 Pulse length: 10s CW Interval: PRI of 10s Total duration: 5 min. MB: Single treatment with in-house cationic gene-carrying bubbles with 1 mg of plasmid DNA and/or TAT peptide; 1-mL sample was infused at 12 mL/h.	Direct readout: Single treatment on day 3 post ligation. RT-qPCR data indicate an approximately 4-fold increase in HGF mRNA compared with untreated controls. Other details: A synergistic effect was found when using MBs contained both TAT peptide and HGF, resulting in a 6.5-fold increase in HGF expression compared with untreated controls (~1.5x more than US + MB without TAT). All analyses were performed on day 10 post ligation (7 days post treatment). MVD was found to modestly increase with gene-carrying MBs compared with US + MBs alone, but represents an approximate factor of 2- to 2.5-fold increase over negative controls.
Ling et al. 2013 ¹⁴²	MSCs/Canine/#6/femoral vein (i.v.)	US system: UTG 1025 Probe/Frequency: 1 MHz Pressure/Power: 0.5–2 W/cm ² Pulse length: 5s (PRF of 1 kHz) Interval: DC of 50% Total duration: 10 min.	Direct readout: None reported. Other details: In study 1, results indicate increased levels of SDF-1, VCAM-1, and VEGF expression at highest power. In study 2, canine MSCs were injected post US treatment and reveals improved myocardial perfusion (assessed via SPECT) and heart function (LVEF, LVIDs, and LVFS) at 4 weeks post treatment.

(Continued on next page)

Table 3. Continued

Author	GOI/Model/Targeted pathway ^a /Injection route	Ultrasound settings	Results summary
		MB: Three treatments with 2 mL of in-house lipid MB (2×10^8 MB/mL) on day 1, 4, and 7 post-myocardial infarction with or without MSCs. Details on infusion speed/time were not provided.	
Yuan et al. 2012 ¹⁴³	HGF/Canine/#1/direct LV injection	US system: UTG 1025 Probe/Frequency: 1 MHz Pressure/Power: 1 W/cm ² Pulse length: 30s (CW) Interval: DC of 75% Total duration: 1 min. MB: Single treatment with in-house lipid bubble (0.1 mL) co-injected with 100 µg of plasmid DNA intramyocardially delivered in 5 locations (total of 0.5 mL of MB and 500 µg of DNA).	Direct readout: None reported. Other details: Single treatment 5 min post ligation. After 28 days, authors observed decreased LV mass, decreased infarct size, and increased MVD. They also observed a 1.8x-fold increase in VEGF levels compared with HGF+US group (no MBs).
Zhong et al. 2012 ¹⁴⁴	MSCs/Canine/#6/femoral vein (i.v.)	US system: UTG 1025 Probe/Frequency: 1 MHz Pressure/Power: 0.5–2 W/cm ² Pulse length: not specified. Interval: DC of 50% Total duration: 10 min. MB: Three treatments with in-house lipid bubbles (2-mL volume at 2×10^8 MB/mL) on days 7, 9, and 11 post-MI. On day 14, MSCs were injected (5 mL at 1.35×10^6 cells/mL). Details on infusion speed/time were not provided.	Direct readout: The number of MSCs increased by 4.57-fold compared with untreated controls, as measured via immunohistochemistry. Other details: Following a single treatment of only US + MBs, mRNA levels of VEGF, SDF-1, VCAM-1, and IL-1b were increased in the infarcted myocardium by a factor of 4x, 5x, 4x, and 5x, respectively, vs. controls.
Fujii et al. 2011 ⁹⁵	SCF, SDF-1 α /Rat/#6/tail vein (i.v.)	US system: Sequoia (Siemens) Probe/Frequency: 15L8 Pressure/Power: MI = 1.6 Pulse length: single frame Interval: every 1.8–2 s in contrast mode Total duration: 20 min. MB: Starting 7 days post ligation, up to 6 treatments with Definity co-incubated with 0.6 mg/kg of plasmid DNA infused at 1.5 mL/h. Heart was scanned from base to apex (3-min cycle)	Direct readout: Levels of SCF protein at 4 weeks post treatment increased statistically by an approximate factor of 1.7 after 6 treatments compared with untreated control, a steady improvement over a single treatment (~1.1x) and three treatments (~1.4x). Similar results were found for SDF-1 α . Other details: On day 24, stem cell homing (as measured via c-kit and CXCR4), and myofibroblast recruitment increased while infarct size decreased with more treatment repeats.
Xu et al. 2010 ¹⁴⁵	MSCs/Rabbit/#6/auricular vein (i.v.)	US system: Vivid 7 (GE) Probe/Frequency: 1.7 MHz Pressure/Power: MI = 1.3 Pulse length: not specified. Interval: every 2 s Total duration: 10 min. MB: At 7 days post-MI, single treatment with in-house lipid bubble (0.1 mL/kg) with or without MSCs. Details on infusion speed/time were not provided.	Direct readout: The number of MSCs increased by 1.45-fold compared with untreated controls, as measured via immunohistochemistry. Other details: Treatment increased MVD (via contrast echocardiography and staining), increased level of VEGF in ischemic myocardium, V-CAM1 expression and improved heart function (LVEF, LVFS) at 4 weeks post treatment.
Fujii et al. 2009 ¹⁴⁶	SCF, VEGF/Mouse/#6, #1/tail vein (i.v.)	US system: Sequoia (Siemens) Probe/Frequency: 15L8; 8 MHz Pressure/Power: MI = 1.6	Direct readout: Measured 14 days post treatment, VEGF and SCF protein within the whole heart were approximately 1.2 and 1.3-fold greater than untreated control.

(Continued on next page)

Table 3. Continued

Author	GOI/Model/Targeted pathway ^a /Injection route	Ultrasound settings	Results summary
		Pulse length: single frame Interval: every 0.5 s in contrast mode Total duration: 20 min. MB: Single treatment 7 days post-MI of Definity incubated with 0.6 mg/kg of plasmid DNA and infusion over 1 min. Heart was scanned from base to apex (3 min cycle)	Other details: Five days after treatment, progenitor recruitment was found to be higher in both treatment groups as compared with control, and MVD was also increased compared with controls on day 14.
Kondo et al. 2004 ⁸⁵	HGF Plasmid/Rat/#1/femoral vein (bubbles), direct LV injection (plasmid)	US system: Sonos 5500 (Philips) Probe/Frequency: S3/1.3 MHz Pressure/Power: MI = 1.8 Pulse length: 3 frames Interval: Triggered every eighth end-systole Total duration: 4 min. MB: Single injection of Optison at 12 mL/h over 5 min combined with LV injection of naked plasmid (1.5 mg)	Direct readout: HGF levels were approximately 3-fold higher in the US + MB group vs. the HGF only group as measured via immunohistology. Other details: At 3 weeks, both LV mass infarct size decreased, while capillary and arterial density increased in treated groups compared with HGF injections alone.
Ischemic heart disease (I/R injury)			
Erikson et al. 2017 ¹⁴⁷	TRAF3IP2, p65, JNK1 Mouse/#3/jugular vein (i.v.)	US system: Sonicator 730 (Mettler Electronics) Probe/Frequency: 1 MHz Pressure/Power: 0.6 W/cm ² Pulse length: Not specified Interval: Not specified Total duration: 15 min. MB: Albumin-based MBs bound to AS-ODN (100 µg) were arterially infused “slowly” over 10 min. Three agents were tested, each binding to either TRAF3IP2, p65, or JNK1 oligo.	Direct readout: Protein levels in the heart of treated mice were significantly lower for all three tested MBs; resulting in approximately a 1.75x, 1.5x, and 1.5x decrease in TRAF3IP2, p65, and JNK1 using their respectively targeted bubbles. Other details: AS-ODN targeting TRAF3IP2, p65, or JNK1 all attenuated I/R-induced myocardial injury (infarct size) at 24 h post delivery.
Mofid et al. 2017 ⁸⁹	S100A6/Rat/#2/jugular vein (i.v.)	US system: Sonos 5500 Probe/Frequency: S12/5 MHz Pressure/Power: 120V Pulse length: single frame Interval: every 10 cardiac cycles Total duration: 30 min. MB: Single pre-treatment with in-house cationic MBs (1 × 10 ⁹ MB) coupled to S100A6 plasmid (500 µg) 2 days prior to I/R infused over 5 min. Infusion speed not provided. Heart was scanned from base to apex.	Direct readout: The authors demonstrate an approximate 8-fold increase in S100A6 within the anterior LV compared with normal myocardium on day 1 post I/R (3 days post treatment). Other details: Increased expression of S100A6 up to 28 days post cardiac I/R, reduced infarct size and improved left ventricular systolic function, with less myocyte apoptosis, attenuated cardiac hypertrophy, and less cardiac fibrosis compared with untreated controls.
Du et al. 2017 ¹⁴⁸	GDF11/Mouse/#6/tail vein (i.v.)	US system: Vivid 7 (GE Healthcare) Probe/Frequency: M3S/1.6 MHz Pressure/Power: MI = 1.3 Pulse length: single frame Interval: ECG triggered every fourth cardiac cycle Total duration: 20 min.	Direct readout: The mRNA levels of GDF11 were about 1.3-fold higher in treated vs. untreated hearts, as measured 9 days post I/R (3 days post treatment). Other details: Treatment effective in old mice (not young mice), whereby it improved cardiac function (LVFS), reduced infarct size, decreased senescence markers (p16, p53), and increased

(Continued on next page)

Table 3. Continued

Author	GOI/Model/Targeted pathway ^a /Injection route	Ultrasound settings	Results summary
		MB: Two treatments (day 3 and 6 post I/R) of in-house gene-carrying cationic lipid bubbles infused at a rate of 1.2 mL/h	proliferation of cardiac stem cell antigen (Sca-1+) cells and homing of endothelial progenitor cells and angiogenesis.
Kwekkeboom et al. 2016 ¹⁴⁹	Antagomir/Mouse/tail vein (i.v.)	US system: Sonos 5500 (Philips) Probe/Frequency: S3 and S12, 1.5, 6 and 7 MHz Pressure/Power: MI = 1.4–1.8, B-mode and Power Doppler mode Pulse length: 1 s Interval: every 5 s Total duration: 15 min. MB: Single treatment with cationic in-house lipid bubbles (2×10^9 MB/mL) conjugated to 0.75 mg/kg of antagomir in 0.1 mL volume. Details on infusion speed/time were not provided.	Direct readout: The authors found an increase in antagomir ranging from 2- to 2.5-fold in US-treated diseased heart as compared with untreated controls, as measured via fluorescence microscopy. Other details: While they show interesting improvement in healthy rodent hearts, no significant differences in functional delivery for I/R hearts. Delivery of antagomir was maximal when using the treatment paradigm with the highest MI and more frequent pulses (Doppler mode with S12 probe).
Yan et al. 2014 ¹⁵⁰	Timp 3/Rat/#5/tail vein (i.v.)	US system: Vivid 7 (GE) Probe/Frequency: M3S/1.6 MHz Pressure/Power: MI = 1.3 Pulse length: single frame Interval: ECG trigger interval of four cardiac cycles Total duration: 20 min. MB: Single treatment of an in-house, targeted lipid agent decorated with MMP2 antibody co-injected (0.4 mL) with naked Timp3 plasmid (0.2 mg/kg) and infused at 1.2 mL/h for 20 min.	Direct readout: Anti-MMP2 microbubble treated groups resulted in an approximate 2.1x increase in TIMP3 protein expression within the scar/border zone at 3 days post treatment as compared with untreated controls. Other details: Non-targeted US treatment still exhibited an increase in TIMP3 protein at 3 days post treatment (~1.6x) All increases in protein levels were no longer present by 3 weeks post treatment. MMP2 and MMP9 activity were reduced, resulting in smaller and thicker infarcts and improved cardiac function (LVEF, LVIDs, LVIDd).
Erikson et al. 2003 ⁸⁸	Antisense TNF- α oligo/Rat/#2/jugular vein (i.v.)	US system: Sonicator 730 (Mettler Electronics) Probe/Frequency: 1 MHz Pressure/Power: 0.6 W/cm ² Pulse length: Not specified. Interval: Not specified. Total duration: 15 min. MB: Either single or triple treatment through i.v. or direct LV injection of in-house albumin-based gene-carrying bubbles (100 μ g) infused at 4 mL/h in a total volume of 1 mL.	Direct readout: There was no significant difference in TNF- α mRNA levels between positive controls and single or triple treated rats when performed via venous administration, but a decrease of ~39% (i.e., ~1.6-fold decrease) in protein level was observed. Other details: The authors also tested direct injection within the LV, with the US-treated groups showing no difference in mRNA but a slightly more attenuated level of TNF- α protein expression (~56.6% decrease). Timing experiments showed that treatment just before I/R was more efficient than just after I/R, as well as lower IL-1 β and ICAM-1 levels.
Cardiomyopathy (CM)			
Qin et al. 2023 ⁹²	Sirt3/Porcine/#5/ear vein (i.v.)	US system: EPIQ 5 (Philips) Probe/Frequency: S5-1 Pressure/Power: MI = 1.2–1.35 Pulse length: single frame Interval: triggered every 4 cardiac cycles Total duration: 30 min. MB: Three treatments using an in-house gene-carrying lipid bubble (no MB concentration given) containing 6–7 mg of plasmid diluted into a 50-mL sample and infused via ear vein at 100 mL/h.	Direct readout: Seven days after treatment, human Sirt3 protein levels were 2.8x higher than in untreated controls. Other details: Short-term assessment performed 7 days post treatment demonstrated decreased levels of ROS. Long-term benefits were determined 2 months after treatment preventing LV thickness and mass increase, as well as decrease in pressure overload associated apoptosis and fibrosis. Protein and mRNA levels of ANP, BNP, and α -SMA were decreased compared with controls 2 months post surgery.

(Continued on next page)

Table 3. Continued

Author	GOI/Model/Targeted pathway ^a /Injection route	Ultrasound settings	Results summary
Gao et al. 2021 ¹⁵¹	FGF21/Mouse/#5/tail vein (i.v.)	US system: Single element Probe/Frequency: 0.5 MHz Pressure/Power: 2W Pulse length: Not specified. Interval: DC of 50% Total duration: 5 min. MB: With a regimen of two times a week for 8 weeks, in-house gene-carrying polymer bubbles (no MB concentration given) were loaded with 100 µg/kg of FGF21. Details on infusion speed/time were not provided.	Direct readout: None reported. Other details: After the 8-week treatment period, the US-treated groups demonstrated a decrease in hypertrophic phenotypes, fibrosis, and apoptosis. Further, an increase in cardiac function (LVEF, LVFS, and E/A ratio) was observed.
Zheng et al. 2020 ¹⁵²	FGF1/Rat/#1/tail vein (i.v.)	US system: Acuson Sequoia 512C (Siemens) Probe/Frequency: 15L8-w/12–14 MHz Pressure/Power: MI = 1.9 Pulse length: single frame Interval: Not specified. Total duration: Not specified. MB: Twice a week for 12 weeks, injections consist of a co-administration of SonoVue (2 × 10 ⁸ MB/mL) with nanoliposomes bound to FGF1 (15 µg/kg). Details on infusion speed/time were not provided.	Direct readout: None reported. Other details: US was applied until bubbles were no longer visible in the LV. After treatment, assessment of cardiac function was performed demonstrating an improved cardiac function (LVEF and LVFS) compared with non-US-treated controls. Further, increase in myocardial capillary density was observed and an improvement in the regional myocardial blood flow, the hemodynamics (LVESP and LVEDP) and the myocardial ultrastructure (using SEM).
Kopeček et al. 2019 ⁶³	AntimiR-23a/Mouse/#2/jugular vein (i.v.)	US system: Sonos 7500 (Philips) Probe/Frequency: S3/1.3 MHz Pressure/Power: MI = 1.0 Pulse length: 4 frames Interval: 1 s Total duration: 20 min. MB: Three treatments consisting of in-house, gene-carrying lipid bubble; 100 µL infusion (@2 × 10 ⁹ MB/mL) containing 35 pmol of antimiR at 0.4 mL/h for 15 min via the jugular vein.	Direct readout: After the 2-week protocol, miR-23a levels were found to have decreased by 43% (i.e., a 1.73-fold decrease) compared with untreated, disease model controls. Other details: CM was induced with phenylephrine, which was delivered daily starting at day 0. Treatments were delivered on days 0, 3, and 7. Treated hearts demonstrated no disease-related increase in cardiac mass on day 7. Also, LVFS was shown to be preserved on day 14. Isolated hearts on day 14 demonstrated a significant decrease in miR-23 compared with non-treated diseased hearts.
Cardiomyopathy (DOX-induced, adriamycin-induced)			
Sun et al. 2020 ¹²¹	miR-21/Mouse/#5/tail vein (i.v.)	US system: Not specified. Probe/Frequency: 0.66 MHz Pressure/Power: MI = 1.6 Pulse length: Not specified. Interval: DC of 50% Total duration: 1 min. MB: Weekly treatments spanning 4 weeks of a co-injection of SonoVue (2 × 10 ⁸ MB/mL) with exosome-encapsulated miR-21 (100 µg; achieved through electroporation) in 0.2 mL. Details on infusion speed/time were not provided.	Direct readout: The authors observed an approximate 4.8-fold increase in miR-21 within the heart tissue of treated mice (US + MB and miR-21 loaded exosomes) as compared with untreated controls. Other details: Assessment of cardiac function performed 28 days post-delivery, demonstrating improved cardiac function (LVEF and E/A ratio) compared with non-treated controls.
Tian et al. 2017 ¹⁵³	MaFGF/Rat/#5/tail vein (i.v.)	US system: Acuson Sequoia 512C (Siemens) Probe/Frequency: 15L8-w/12–14 MHz	Direct readout: None reported. Other details: Hearts were treated until bubbles were

(Continued on next page)

Table 3. Continued

Author	GOI/Model/Targeted pathway ^a /Injection route	Ultrasound settings	Results summary
		Pressure/Power: Not specified. Pulse length: 10s Interval: 1s off-interval. Total duration: 33s MB: Co-injection of SonoVue (2×10^8 MB/mL) with in-house gene-loaded nanoliposomes (3 μ g/kg of MaFGF) in 1 mL via the caudal vein over 6 weeks with two treatments weekly. Details on infusion speed/time were not provided.	no longer visible. Prevention of disease-related cardiac physiology (HW/BW) and dysfunction (LVEF, LVFS, LVIDD, LVIDs) was observed post-final treatment. Disease-associated oxidative stress, fibrosis, and apoptosis were shown to be attenuated in treated samples. An increased expression of anti-apoptotic proteins (pAkt and Bcl-2), as well as the decreased expression in pro-apoptotic protein (Bax) were also observed.
Chen et al. 2015 ¹²³	GLP-1/Rat/#5/not specified (i.v.)	US system: Sonos 5500 (Philips) Probe/Frequency: S3/1.3 MHz Pressure/Power: MI = 1.4–1.5 Pulse length: 4 frames Interval: ECG triggered every 4 cardiac cycles Total duration: Not specified. MB: Treatment regime consisted of a 2-week window with three treatments per week using an in-house gene-carrying lipid bubble; each injection consisted of 50 nmol/kg of plasmid. Details on infusion speed/time were not provided.	Direct readout: Levels of GLP-1 mRNA exhibit an 84-fold increase in US-treated hearts vs. control rat hearts (these are healthy hearts that did not express any GLP-1). Other details: A secondary experiment delivered GLP-1 and treated 2 weeks after adriamycin-induced CM to determine recovery potential. A decrease of CM-associated phenotypes (LV mass and wall thickness) and improved cardiac function (LVFS) were observed in both treatments. As well, regeneration and proliferation of adult cardiomyocytes were evident in treated hearts.
Lee et al. 2014 ⁹¹	Survivin/Rat/#3/not specified (i.v.)	US system: Sonos 5500 (Philips) Probe/Frequency: S12/5 MHz Pressure/Power: 120V Pulse length: single frame Interval: every 10 cardiac cycles Total duration: 5 min. MB: Single treatment with in-house, gene-carrying lipid bubbles via a 1-mL volume (10^9 MB with 500 μ g DNA) infused over 5 min. Heart was scanned from base to apex.	Direct readout: At 7 days post treatment, survivin expression increased by approximately 2.8-fold in treated vs. untreated hearts. Other details: Increased expression of survivin lasted for up to 3 weeks post delivery. Improved cardiac function (LVFS and LVEDV) and decrease in fibrosis was demonstrated 3 weeks post-delivery compared with non-treated hearts. As well, a decrease in disease-associated apoptosis was observed 1 week post-delivery in surviving-treated hearts.
Heart transplant rejection			
Wang et al. 2020 ¹²⁰	Galectin-7/Rat/#5/tail vein (i.v.)	US system: Not specified Probe/Frequency: 1 MHz Pressure/Power: 0.8 MPa/2 W/cm ² Pulse length: Not specified. Interval: DC of 50% Total duration: 2 min. MB: Four treatments of in-house, gene-carrying lipid bubbles of 200 μ L (0.39 nmol of siRNA per MB; no MB concentration given). Treatment performed 30 s after injection. Details on infusion speed/time were not provided.	Direct readout: Three days post-treatment regimen, galectin-7 levels were about a factor of 2 lower in treated hearts compared with controls, as measured both by immunofluorescence and RT-qPCR. Other details: No significant reduction in galectin-7 levels was found in non-heart issue. A decrease in apoptotic cells and immune cell penetration, indicating prevention of rejection, was also observed.
Yi et al. 2020 ¹²²	Anti-miR-155/Mouse/#5/not specified (i.v.)	US system: Sonitron 2000 (Nepa Gene) Probe/Frequency: 2 MHz Pressure/Power: 2W/cm ²	Direct readout: On day 7 post transplant, mRNA levels of miR-155 in treated hearts dropped to 40% of native levels (i.e., a 2.5-fold decrease) as compared with untreated controls.

(Continued on next page)

Table 3. Continued

Author	GOI/Model/Targeted pathway ^a /Injection route	Ultrasound settings	Results summary
		Pulse length: Not specified. Interval: DC = 50% Total duration: 2 min. MB: Three treatments (day 1, 3, and 5 after transplant) consisting of in-house, gene-carrying lipid bubbles. Volume administered was 150 μ L (@ 2×10^9 MB/mL) with 0.8 nmol of antimiR. Details on infusion speed/time were not provided.	Other details: Anit-miR-155 delivered with US also ensured a longer survival of allograft heart compared with non-US controls. Treated hearts also demonstrated reduced expression of inflammatory cytokines (e.g., IL-6) up to 7 days after heart transplant.
Fibrosis			
Feroze et al. ¹⁵⁴	miR-29b mimic/Mouse/jugular vein (i.v.)	US system: Sonos 7500 (Philips) Probe/Frequency: S3/1.3 MHz Pressure/Power: MI = 1.0 Pulse length: 4 frames Interval: 1s Total duration: 20 min. MB: Three treatments of in-house, gene-carrying lipid bubble (4×10^8 MB/mL) consisting of 3.5×10^{-8} μ g/MB of miR at 1.2 mL/h for 15 min.	Direct readout: One day after a single treatment, there was a 2.26-fold increase of miR-29b expression within the heart in the treatment cohort vs. sham-treated controls. Other details: After three treatments, fibrotic transcripts and α -SMA levels were lower in the treated vs. sham groups. Heart physiology was also improved in the treatment groups. Echo data confirming a decrease in LVED volume and an increase in fractional shortening and ejection fraction were confirmed on day 10.
Li et al. 2023 ¹⁵⁵	Gal-3/Rat/#4/not specified	US system: Sonitron 2000 (Nepa Gene) Probe/Frequency: 1 MHz Pressure/Power: 2 W/cm ² Pulse length: Not specified. Interval: DC of 50% Total duration: 20 min. MB: Three treatments (day 1, 3, and 7 post-operation) using an in-house, gene-carrying lipid bubble of a volume of 500 μ L consisting of 120 μ g of Gal-3 shRNA and infused over 20 min. Details on infusion speed were not provided.	Direct readout: The authors observed a 3x and 5x decrease in native Gal-3 mRNA levels at 7 and 21 days post MI, respectively. Other details: Gal-3 protein levels did not change by day 7, and were significantly lower by day 21. LVEF, LVFS, LVIDD, and LVIDs were elevated by 21 days compared with untreated controls, as measured by echo.
Coronary microembolization (CME)			
Su et al. 2015 ¹⁵⁶	miR-21/Pig/#5/marginal ear vein (i.v.)	US system: Not specified. Probe/Frequency: 1 MHz Pressure/Power: 2 W/cm ² Pulse length: 10s Interval: DC of 50% Total duration: 20 min. MB: Single treatment with in-house, gene-carrying lipid bubble at a volume of 6 mL infusion consisting of 2 mg mL ⁻¹ of plasmid. Details on infusion speed/time were not provided.	Direct readout: There was a 4.48-fold increase in miR-21 within the heart of treated pigs vs. control. Other details: Nine hours post-CME introduction improved cardiac function (LVEF, LVIDD, LVFS, and CO) was shown compared with CME group. As well, a lower expression of gene associated with CME induced inflammation (PDCC4/NF- κ B/TNF- α).

BW, body weight; CO, cardiac output; CX43, connexin-43; DC, duty cycle; E/A, mitral ratio of peak early to late diastolic filling velocity; Gal-3, galectin-3; GOI, gene of interest; HGF, hepatocyte growth factor; HW, heart weight; LVAWd, LV anterior wall thickness in diastole; LVEDP, LV end-diastolic pressure; LVEDV, LV end-diastolic volume; LVEF, LV ejection fraction; LVESP, LV end-systolic pressure; LVFS, fractional shortening; LVIDD, left ventricular internal dimension-diastole; LVIDs, left ventricular internal dimension-systole; MaFGF, Mutant acidic fibroblast growth factor; MB, microbubble; MSC, mesenchymal stem cells; MVD, microvascular density; PHD2, prolyl hydroxylase-2; PRF, pulse repetition frequency; PRI, pulse repetition interval; ROS, reactive oxygen species; SCF, stem cell factor; SEM, scanning electron microscopy; Sirt3, sirtuin-3; TAT, trans-activating transcriptional activator; TIMP3, TIMP metalloproteinase inhibitor 3; TNF- α , tissue necrosis factor; TRAF3IP2, TRAF interaction protein 2.

^aTargeted pathways as defined in Table 2.

protocol for 15 min, they compared their treatment approach using albumin-coated bubbles carrying the ODN in two different scenarios: 24 h before I/R, and treatment during the first 15 min of reperfusion. With either a single treatment or a multiple treatment strategy (three treatments daily for 3 consecutive days), the authors found an approximate 40% decrease in protein levels of TNF- α while observing no significant change in mRNA expression with treatment 24 h before I/R injury. With similar findings in each scenario (before or after I/R injury), the authors found a much stronger therapeutic effect with direct injection of ODN-bound bubbles within the LV, observing decreases on the order of 70–75% in this manner. Importantly, the decreased expression of TNF- α significantly inhibited other post-ischemic inflammatory mediators on both the protein and mRNA level, including ICAM-1 and IL-1 β .

More recently, robust work by Mofid et al.⁸⁹ confirmed successful functional delivery of S100A6 plasmid in a rodent model of I/R, highlighting that cardiac overexpression of this gene leads to improved myocardial perfusion injury and LV function. Indeed, S100A6 is a key Ca²⁺-binding protein that plays a role in many cellular processes, including cell proliferation, differentiation, cardiomyocyte contractility, hypertrophy, and apoptosis. In this work, the authors coupled either S100A6 plasmid or an empty plasmid (as a control) to cationic lipid microbubbles at a dose of 500 μ g per 10⁹ bubbles. With a 5-min injection of the DNA-microbubble complexes via the jugular vein, high-powered ultrasound was delivered via a Sonos 5500 Philips system using an S12 transducer at a frequency of 5 MHz placed along the short axis of the LV. The probe was slowly moved from the base to the apex of the heart to increase dose deposition, and the total treatment duration was 30 min. Treatment was performed 48 h before I/R injury, and the data highlights increased expression of S100A6 in the anterior LV of S100A6-treated rats up to 28 days after I/R induction, with an 8-fold increase in expression at day 1 that decreased over time. Additionally, LVEF and fractional area assessed through echocardiography progressively improved in treated rats compared with control up to day 28, with markedly smaller scar tissue regions (approximately 2-fold less).

Cardiomyopathies

Cardiomyopathy (CM) refers to a heterogeneous group of diseases that cause abnormalities in the myocardium resulting in impaired cardiac activity,⁹⁰ including dilated CM, hypertrophic CM, restrictive CM, and CM caused as a side effect of known cancer therapeutics (e.g., doxorubicin-induced CM). An early example of using ultrasound-mediated cardiac gene delivery for this application was shown in a study by Lee et al.,⁹¹ in which a survivin gene plasmid was delivered to a doxorubicin-induced cardiomyopathic rodent model. Survivin is a gene recognized for its ability to inhibit apoptosis, and the motivation for its targeted delivery is that this would help prevent disease-related cell death and thus LV systolic dysfunction. The study utilized a cationic microbubble formulation bound with a survivin plasmid to perform a single delivery 3 weeks after beginning doxorubicin injection. Treatment was conducted using an S12 transducer from a Philips Sonos 5500 ultrasound system, positioned transversely

over the heart at the mid-papillary level while slowly sweeping. A frequency of 5 MHz and 120 V power was utilized for 5 min with a pulsing interval of 10 cardiac cycles during infusion of the plasmid bound bubbles. This therapeutic gene was confirmed to successfully reach the cardiomyocytes and significantly increased expression 1 week post-delivery (4 weeks after beginning doxorubicin). The cardiovascular therapeutic benefit was clearly demonstrated with decreased apoptosis and fibrosis observed 1 week post-delivery, and improved cardiac function (LVEDV and LVFS) 3 weeks post-delivery.

In comparison, one of the more recent examples of this technique being used for cardiomyopathy is shown in a study by Qin and colleagues.⁹² The gene of focus is Sirt3, which has been shown to have antioxidative activity and regulate hypertrophy. A Sirt3 plasmid bound to a cationic bubble formulation was employed and delivered to a pathological hypertrophy porcine model. Here, the treatment protocol takes advantage of the non-invasive nature of ultrasound-mediated delivery to perform multiple treatments. This therapeutic gene is delivered three times with one day intervals, and treatment was done using an S5-1 transducer on a Philips EPIQ5 ultrasound system, with an MI of 1.2–1.35 triggered every four diastolic cardiac cycles for a 30-min period throughout the infusion of the plasmid-microbubble solution. Repression of hypertrophic phenotypes was observed at 7 days and as long as 2 months after final treatment, including inhibition of disease-related conditions such as cardiac enlargement, fibrosis, and apoptotic activity. This study also analyzed organs such as kidneys, livers, and lungs for any potential damage associated with the treatments. However, no impact was shown, thereby highlighting the spatial specificity and safety from off-target effects.

Though both studies look at different therapeutic genes and different forms of cardiomyopathy, they both provide robust evidence of the efficiency and capability of ultrasound-mediated delivery to this class of disease. These examples highlight effective therapy with plasmids, but other therapeutics have been used with success, including miRNA and even small proteins (Table 3).

OUTLOOK AND FUTURE DIRECTIONS

Global summary

The wide array of treatment parameters, in terms of ultrasound (e.g., system, sequences, duration), dosing (e.g., microbubble concentration and injection details, gene concentration), readouts (e.g., mRNA, protein, physiological), and disease model make comparisons between all studies (Table 3) a non-trivial matter. However, some general trends within the field of cardiac gene delivery using ultrasound can be proposed, as we have summarized in Figure 3. This figure attempts to quantify the effectiveness of gene delivery through the metric of “direct readout,” which is, when reported, a direct measure within the diseased heart of the genetic material delivered via ultrasound and microbubbles as compared with a control, untreated diseased cohort (i.e., the negative controls within the respective study), here demarked as a fold-change. Indirect measures of therapeutic efficiency, including physiological improvements of the diseased heart,

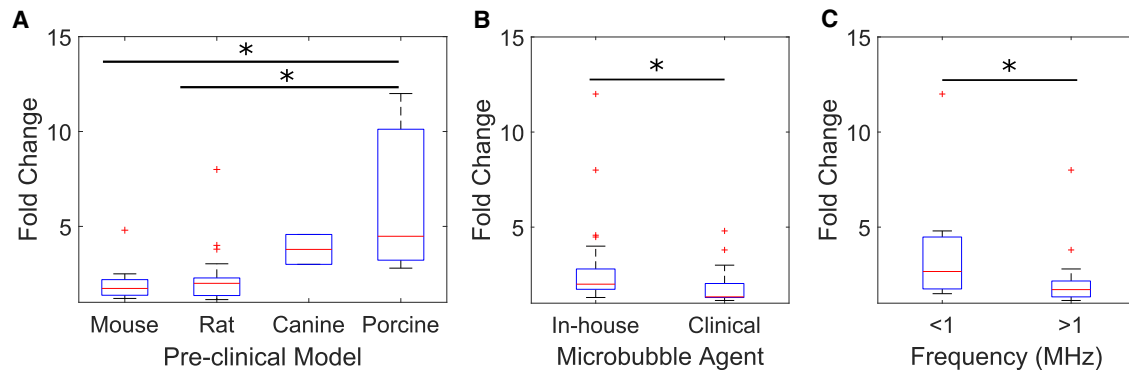


Figure 3. Aggregate data from all reported studies depicting a measurement of “direct readout,” which is—when available—a relative measure of the delivered gene product within the diseased heart of ultrasound-treated vs. control groups

The central red line within each box marks the median, and the bottom and top edges mark the 25th and 75th percentile, respectively. The whiskers extend to the most extreme data points not considered outliers, while the red plus signs indicate data outliers. There is a notable trend of increasing cardiac gene delivery efficiency with (A) increasing size of the preclinical model ($p < 0.02$), (B) when custom, in-house microbubbles were employed compared with clinical ones ($p < 0.02$), and (C) when the transmit frequency was kept at or below 1 MHz ($p = 0.008$).

and downstream cytokine or protein expression, are not possible to compare due to the distinct differences in model disease and heterogeneity/sparsity of their measurements. As shown in Figure 3A, there is a general trend of increasing delivery efficiency in larger preclinical models, with a median fold-change in delivery of 1.7, 2.0, 3.8, and 4.5 in mice, rats, canines, and pigs, respectively ($p < 0.02$ between pigs vs. rats, and $p < 0.02$ for pigs vs. mice). Indeed, many of these studies use clinical systems with clinical frequencies, and thus the acoustic beam is more compatible with human-sized anatomy. This suggests that as this technique scales up to the clinical area, it will only serve to strengthen the direct and targeted therapeutic delivery efficiency. There is also a slight increase in gene delivery efficiency reported in studies using in-house, usually lipid-based bubbles compared with commercially available, clinical agent (2.0 vs. 1.33; $p < 0.02$) (Figure 3B). Indeed, in the few studies that directly compared these two types of agent, gene-loaded in-house agents yielded slightly higher efficiencies.⁹⁵ There is however a strong correlation with transmit frequency, with studies using at or below 1 MHz ($f \leq 1$) yielding more effective cardiac gene delivery than those above ($f > 1$) – 2.7 vs. 1.7 ($p = 0.008$) (Figure 3C). While higher transmit frequencies would bring imaging resolution more in line with anatomical length scale in the smaller preclinical models, microbubble response (and thus gene delivery potential) does not scale in the same manner, owing to their nonlinear and resonance response.^{2,33,94} It is important here to note that, while not evident within this aggregate data summary, studies in which multiple, repeated treatments were performed do suggest prolonged gene expression as compared with single-treatment paradigms.⁹⁵

Molecularly targeted contrast microbubbles

While conventional microbubbles are used clinically for routine contrast imaging, there is another class of contrast microbubbles that are designed to adhere to specific molecules or cells within the vascular system. Typically, these are synthesized via conjugation of

disease-targeting ligands (e.g., antibodies, peptides) to the surface of the bubbles. The disease-specific retention of contrast bubbles, which ultimately provides a disease-specific contrast-enhanced echo, has many applications from assessing spatial/temporal patterns of expression and disease progression, to evaluating and optimizing new therapies, to early diagnosis of disease, and to monitor disease progression. Indeed, robust research using these molecularly targeted microbubbles in atherosclerosis and ischemia-based imaging preclinical applications have demonstrated selective imaging of VCAM-1,⁹⁶ ICAM-1,^{97,98} and P-selectin.^{99,100} Recently, the first targeted microbubble agent selective for VEGFR has been translated into humans for cancer detection, the initial results of which were published in 2010.¹⁰¹ With respect to cardiovascular applications, there is an ongoing trial (NCT03009266) investigating a commercially available agent and its use toward selective imaging of ischemic memory.¹⁰²

There is some preclinical evidence that molecularly targeted microbubbles can further be made to carry a genetic payload and used to improve gene delivery as compared with more traditional, non-targeted agent. Within the context of CVD, Xie and colleagues⁵⁷ were perhaps one of the first to show that endothelial targeting (via P-selectin and ICAM-1) of gene-carrying microbubbles was feasible, and in fact increased the gene efficiency by 5-fold at a modest MI of 0.6 in a murine model of hindlimb ischemia compared with non-targeted control bubbles. Zhou et al.¹⁰³ demonstrated a similar result, using ICAM-1 targeted microbubbles to deliver Ang1 in a rabbit model of myocardial infarction, which resulted in an approximate 3-fold increase in delivery efficiency compared with non-targeted bubbles using a Philips iE33 system in contrast mode at 1.7 MHz and an MI of 1.3.

Microbubble-assisted vascular gene delivery

While this review focuses on delivery to the heart, it is important to note that there has been exciting progress in ultrasound-assisted

gene delivery for vascular therapy in peripheral tissues. In one of the earlier studies in this area, Takeuchi et al.¹⁰⁴ investigated ultrasound-mediated potentiation of C-type natriuretic peptide (CNP) in a rat carotid artery balloon injury model to prevent neointimal hyperplasia. They employed a co-infusion approach of CNP with commercially available Optison agent, with 10-min-long treatments repeated five times at 3-min intervals using a clinical probe at 1.8 MHz and an MI of 1.0. Their results indicated that ultrasound-mediated delivery of CNP markedly reduced the intima/media ratio to 18% of that of the control rats, which persisted for 28 days post-injury, and resulted in a drastic decrease in the dose requirement of CNP (10x decrease).

Direct gene delivery of an otherwise impermeable plasmid was first demonstrated in a rodent model of hindlimb ischemia by Leong-Poi and colleagues⁸ through administration of a cationic microbubble formulation coupled to VEGF165 plasmid continuously infused for 10 min. Using a Philips Sonos 5500 system at 1.3 MHz, treatment was performed for 20 min while gradually sweeping the probe along the length of the proximal hindlimb muscles. In this work, the authors convincingly demonstrate through contrast ultrasound imaging and confocal microscopy that VEGF-treated hindlimb exhibited increased muscle perfusion and vascular density at 2 weeks post treatment (4 weeks post surgery) with partial regression at 6 weeks. Further, they showed using GFP plasmid that gene delivery was localized within the vascular endothelium of both arterioles and capillaries, as well as evidence of delivery to adjacent cardiomyocytes. Since then, there have been a handful of other studies investigating ultrasound-assisted delivery of plasmids to peripheral tissues for vascular gene therapy, including VEGF,^{105,106} Ang-1,¹⁰⁷ SDF-1,¹⁰⁸ and microRNA.¹⁰⁹

Microbubble-mediated CVD gene modulation without gene delivery

As previously mentioned, it has long been observed that contrast agent microbubbles under specific acoustic conditions are able to permeate blood vessels.³⁹ It was hypothesized soon thereafter that this local blood vessel rupture might stimulate the growth and remodeling of neovessels via natural repair mechanisms,^{110,111} without the need to deliver an exogenous compound. In these studies, standard ultrasound-enhancing microbubbles were used in conjunction with a single-element transducer at 1 MHz. Treatment consisted of 0.1 s of ultrasound every 5 s to either healthy or occluded rat skeletal muscle at an MI ranging from 0.5–0.75 for 1 min. The results highlight that, compared with non-treated controls, stimulating the muscle with ultrasound and microbubbles resulted in increased lateral hyperemia blood flow and density of smooth muscle cell α -actin positive vessels up to 14 days post treatment. Subsequent work investigating the molecular underpinnings of this approach using a mouse model of limb ischemia revealed increased levels of VEGF and recruitment of leukocytes (e.g., macrophages and T cells).¹¹²

With the concept of microbubble-induced angiogenesis as a basis, more recent work has demonstrated this technique toward reversing cardiac dysfunction in an animal model of diabetic cardiomyopa-

thy.^{113,114} Using clinical SonoVue agent, a commercial scanner (VINNO 70, 4 MHz, 8–36 cycles, DC = 60%, 20 min duration) aimed directly at the heart improved reparative neovascularization, and increased cardiac perfusion was observed in a rat model of this disease.¹¹³

Perspectives

Targeted delivery of molecular therapeutics using ultrasound has tremendous potential for cardiac gene delivery. While met with exciting preclinical success, it is important to acknowledge its limitations. First, the results summarized here demonstrate modest transfection efficiency, notably in comparison with viral methods. Given the non-invasive and localization potential of this method, this challenge can be mitigated by repeat injections, as well as the development of more efficient molecular therapeutics, e.g., in combination with CRISPR-Cas9 approaches.¹¹⁵ Second, the mechanisms of this approach are not fully elucidated, particularly the way in which intravascular microbubbles deliver the payload to extravascular target tissue. To this end, there are many ongoing investigations exploring this concept in both cardiac and oncology contexts.^{44,53,116} Indeed, comparisons of gene quantification using this natively intravenous approach vs. direct intramyocardial injection has not been thoroughly addressed but would be a useful measure to appreciate the efficiency of ultrasound-assisted cardiac gene delivery. Further elucidation of this concept will drive modulation of the approach itself (e.g., pulse parameters, microbubble concentration) toward improving the delivery efficiency.

With a view toward advancing the technique of cardiac gene delivery using ultrasound there are numerous factors that need optimization. First, the summarized data in Figure 3B suggest that, generally speaking, incorporation of the gene construct with a cationic bubble agent results in increased transfection compared with co-injection. What is less clear, however, is the amount of gene dosing in these studies. Quantification of the mass of molecular therapeutic that remains bound to the microbubble solution post-synthesis (i.e., how efficient the loading process is) is not often reported. Further, synthesis of in-house cationic agent is sensitive to agent handling, and the resulting effects on microbubble formulation and size distribution play a large role in the efficiency of gene loading and overall gene capacity. Indeed, even if the same dose of microbubble-bound therapeutic is administered, slight differences in bubble size distribution and *in vivo* stability will change the available concentration of gene construct to be deposited. Herein lies the major advantage of using a co-injection strategy with clinical agent, whereby the dose of injected gene construct, along with the bubble agent characteristics and resulting acoustic physics are well documented and more reproducible.

In terms of ultrasound transmit conditions, perhaps the most direct approach is the use of clinical scanners around 1–2 MHz. Here, image-guided delivery is possible via standard contrast-enhanced modes, and parameters for the disruption-replenishment techniques including acoustic power and number of burst frames can be

modified. The real-time visualization of contrast perfusion helps confirm agent and injection reproducibility, and treatment pulses can be triggered either manually or externally to allow microbubbles to replenish the target cardiac tissue. Given the imaging nature of these scanners, a drawback of this technique is the inability to modify the pulse length itself, which is fixed to diagnostic pulses. However, recent technical advancements have been employed to modify commercial transducer probes to incorporate longer duration pulses (up to 20 μ s).¹¹⁷ Further, a subset of the studies using clinical probes in Table 3 translated the probe position during therapy to ensure complete treatment of the heart. While this may not be necessary in applications in which the focal volume of the acoustic beam is size-matched to the region of the interest within the heart, it will likely be required for translation within the clinical arena.

Concluding remarks

With the recent clinical successes of gene therapy, including seven FDA-approved products and several hundred more in the final stages of the clinical approval pipeline, research into cardiac gene therapy is on the rise.⁶ Given that the gene delivery approach plays a critical role in gene therapy efficiency, ultrasound-mediated gene delivery, which uses ultrasound-stimulated microbubbles, is an exciting and emerging methodology. Indeed, this technique is an inherently image-guided approach that can be performed using both clinical scanners and clinical agents—facilitating its translation into clinical practice—notably in diagnostic situations in which echocardiography is the standard of care. While there is still more fundamental work to be explored, including optimal therapeutic protocols (e.g., injection timing, relevant dose, high MI parameters), selection of molecular therapeutic, and perhaps the design of new therapeutic transducers or non-viral acoustically sensitive vectors, the tremendous advancements that have been demonstrated in preclinical models to date reinforce the idea that translation of contrast echocardiography-mediated localized cardiac gene delivery is a feasible near-term objective.

ACKNOWLEDGMENTS

This work was supported by the Canada Research Chairs program (CRC-2023-00137), Canadian Cardiovascular Society (1512960), and Canadian Institutes of Health Research (496216). B.H. is also a Burroughs Wellcome Fund fellow (BWF-CASI; 1018212.03).

AUTHOR CONTRIBUTIONS

D.S., E.M., S.H., H.Y., and B.H. wrote the manuscript. D.S. and B.H. edited the manuscript. B.H. obtained the funding.

DECLARATION OF INTERESTS

The authors declare no competing interests.

REFERENCES

- Yusefi, H., and Helfield, B. (2022). Ultrasound Contrast Imaging : Fundamentals and Emerging Technology. *Front. Physiol.* *10*, 1–16. <https://doi.org/10.3389/fphys.2022.791145>.
- Kooiman, K., Roovers, S., Langeveld, S.A.G., Kleven, R.T., Dewitte, H., O'Reilly, M.A., Escoffre, J.M., Bouakaz, A., Verweij, M.D., Hynynen, K., et al. (2020). Ultrasound-Responsive Cavitation Nuclei for Therapy and Drug Delivery. *Ultrasound Med. Biol.* *46*, 1296–1325. <https://doi.org/10.1016/j.ultrasmedbio.2020.01.002>.
- Lipsman, N., Meng, Y., Bethune, A.J., Huang, Y., Lam, B., Masellis, M., Herrmann, N., Heyn, C., Aubert, I., Boutet, A., et al. (2018). Blood-brain barrier opening in Alzheimer's disease using MR-guided focused ultrasound. *Nat. Commun.* *9*, 2336. <https://doi.org/10.1038/s41467-018-04529-6>.
- Tsao, C.W., Aday, A.W., Almarzooq, Z.I., Alonso, A., Beaton, A.Z., Bittencourt, M.S., Boehme, A.K., Buxton, A.E., Carson, A.P., Commodore-Mensah, Y., et al. (2022). Heart Disease and Stroke Statistics-2022 Update: A Report from the American Heart Association. *Circulation* *145*, e153–e639. <https://doi.org/10.1161/CIR.0000000000001052>.
- Matkar, P.N., Leong-Poi, H., Singh, K.K., and Singh, K.K. (2016). Cardiac gene therapy: Are we there yet? *Gene Ther.* *23*, 635–648. <https://doi.org/10.1038/gt.2016.43>.
- Cannatà, A., Ali, H., Sinagra, G., and Giacca, M. (2020). Gene Therapy for the Heart Lessons Learned and Future Perspectives. *Circ. Res.* *126*, 1394–1414. <https://doi.org/10.1161/CIRCRESAHA.120.315855>.
- Chen, H.H., Matkar, P.N., Afrasiabi, K., Kuliszewski, M.A., and Leong-Poi, H. (2016). Prospect of ultrasound-mediated gene delivery in cardiovascular applications. *Expet Opin. Biol. Ther.* *16*, 815–826. <https://doi.org/10.1517/14712598.2016.1169268>.
- Leong-Poi, H., Kuliszewski, M.A., Lekas, M., Sibbald, M., Teichert-Kuliszewska, K., Klibanov, A.L., Stewart, D.J., and Lindner, J.R. (2007). Therapeutic arteriogenesis by ultrasound-mediated VEGF165 plasmid gene delivery to chronically ischemic skeletal muscle. *Circ. Res.* *101*, 295–303. <https://doi.org/10.1161/CIRCRESAHA.107.148676>.
- Carson, A.R., McTiernan, C.F., Lavery, L., Grata, M., Leng, X., Wang, J., Chen, X., and Villanueva, F.S. (2012). Ultrasound-targeted microbubble destruction to deliver siRNA cancer therapy. *Cancer Res.* *72*, 6191–6199. <https://doi.org/10.1158/0008-5472.CAN-11-4079>.
- McMahon, D., O'Reilly, M.A., and Hynynen, K. (2021). Therapeutic Agent Delivery across the Blood-Brain Barrier Using Focused Ultrasound. *Annu. Rev. Biomed. Eng.* *23*, 89–113. <https://doi.org/10.1146/annurev-bioeng-062117-121238>.
- Isner, J.M., Pieczek, A., Schainfeld, R., Blair, R., Haley, L., Asahara, T., Rosenfield, K., Razvi, S., Walsh, K., and Symes, J.F. (1996). Clinical evidence of angiogenesis after arterial gene transfer of phVEGF165 in patient with ischaemic limb. *Lancet* *348*, 370–374. [https://doi.org/10.1016/S0140-6736\(96\)03361-2](https://doi.org/10.1016/S0140-6736(96)03361-2).
- Losordo, D.W., Vale, P.R., Symes, J.F., Dunnington, C.H., Esakof, D.D., Maysky, M., Ashare, A.B., Lathi, K., and Isner, J.M. (1998). Gene Therapy for Myocardial Angiogenesis. Initial clinical results with direct myocardial injection of phVEGF165 as sole therapy for myocardial ischemia. *Circulation* *98*, 2800–2805.
- Anttila, V., Saraste, A., Knuuti, J., Hedman, M., Jaakkola, P., Laugwitz, K.L., Krane, M., Jeppsson, A., Sillanmäki, S., Rosenmeier, J., et al. (2023). Direct intramyocardial injection of VEGF mRNA in patients undergoing coronary artery bypass grafting. *Mol. Ther.* *31*, 866–874. <https://doi.org/10.1016/j.ymthe.2022.11.017>.
- Ylä-Herttuala, S., and Martin, J.F. (2000). Cardiovascular gene therapy. *Lancet* *355*, 213–222.
- Ylä-Herttuala, S., Bridges, C., Katz, M.G., and Korpisalo, P. (2017). Angiogenic gene therapy in cardiovascular diseases: Dream or vision? *Eur. Heart J.* *38*, 1365–1371. <https://doi.org/10.1093/eurheartj/ehw547>.
- Rincon, M.Y., VandenDriessche, T., and Chuah, M.K. (2015). Gene therapy for cardiovascular disease: Advances in vector development, targeting, and delivery for clinical translation. *Cardiovasc. Res.* *108*, 4–20. <https://doi.org/10.1093/cvr/cvv205>.
- Hammond, H.K., Penny, W.F., Traverse, J.H., Henry, T.D., Watkins, M.W., Yancy, C.W., Sweis, R.N., Adler, E.D., Patel, A.N., Murray, D.R., et al. (2016). Intracoronary gene transfer of adenylyl cyclase 6 in patients with heart failure: A randomized clinical trial. *JAMA Cardiol.* *1*, 163–171. <https://doi.org/10.1001/jamacardio.2016.0008>.
- Zacchigna, S., Zentilin, L., and Giacca, M. (2014). Adeno-associated virus vectors as therapeutic and investigational tools in the cardiovascular system. *Circ. Res.* *114*, 1827–1846. <https://doi.org/10.1161/CIRCRESAHA.114.302331>.
- St George, J.A. (2003). Gene therapy progress and prospects: Adenoviral vectors. *Gene Ther.* *10*, 1135–1141. <https://doi.org/10.1038/sj.gt.3302071>.

20. Karvinen, H., Pasanen, E., Rissanen, T.T., Korpisalo, P., Vähäkangas, E., Jazwa, A., Giacca, M., and Ylä-Herttua, S. (2011). Erratum: Long-term VEGF-A expression promotes aberrant angiogenesis and fibrosis in skeletal muscle. *Gene Ther.* 18, 1180. <https://doi.org/10.1038/gt.2011.93>.
21. Allen, T.M., and Cullis, P.R. (2013). Liposomal drug delivery systems: From concept to clinical applications. *Adv. Drug Deliv. Rev.* 65, 36–48. <https://doi.org/10.1016/j.addr.2012.09.037>.
22. Kulkarni, J.A., Cullis, P.R., and Van Der Meel, R. (2018). Lipid Nanoparticles Enabling Gene Therapies: From Concepts to Clinical Utility. *Nucleic Acid Therapeut.* 28, 146–157. <https://doi.org/10.1089/nat.2018.0721>.
23. Zimmermann, T.S., Lee, A.C.H., Akinc, A., Bramlage, B., Bumcrot, D., Fedoruk, M.N., Harborth, J., Heyes, J.A., Jeffs, L.B., John, M., et al. (2006). RNAi-mediated gene silencing in non-human primates. *Nature* 441, 111–114. <https://doi.org/10.1038/nature04688>.
24. Cullis, P.R., and Hope, M.J. (2017). Lipid Nanoparticle Systems for Enabling Gene Therapies. *Mol. Ther.* 25, 1467–1475. <https://doi.org/10.1016/j.jymthe.2017.03.013>.
25. Ilahibaks, N.F., Lei, Z., and Sluijter, J.P.G. (2024). Extracellular vesicles as vehicles for drug delivery to the heart. *Eur. Heart J.* 3, ehae099. <https://doi.org/10.1093/eurheartj/ehae099>.
26. Sahoo, S., Adamiak, M., Mathiyalagan, P., Kenneweg, F., Kafert-Kasting, S., and Thum, T. (2021). Therapeutic and Diagnostic Translation of Extracellular Vesicles in Cardiovascular Diseases: Roadmap to the Clinic. *Circulation* 143, 1426–1449. <https://doi.org/10.1161/CIRCULATIONAHA.120.049254>.
27. Li, X., La Salvia, S., Liang, Y., Adamiak, M., Kohlbrenner, E., Jeong, D., Chepurko, E., Ceholski, D., Lopez-Gordo, E., Yoon, S., et al. (2023). Extracellular Vesicle-Encapsulated Adeno-Associated Viruses for Therapeutic Gene Delivery to the Heart. *Circulation* 148, 405–425. <https://doi.org/10.1161/CIRCULATIONAHA.122.063759>.
28. Song, Y., Zhang, C., Zhang, J., Jiao, Z., Dong, N., Wang, G., Wang, Z., and Wang, L. (2019). Localized injection of miRNA-21-enriched extracellular vesicles effectively restores cardiac function after myocardial infarction. *Theranostics* 9, 2346–2360. <https://doi.org/10.7150/thno.29945>.
29. Nawaz, M., Heydarkhan-Hagvall, S., Tangruksa, B., González-King Garibotti, H., Jing, Y., Maugeri, M., Kohl, F., Hultin, L., Reyahi, A., Camponeschi, A., et al. (2023). Lipid Nanoparticles Deliver the Therapeutic VEGFA mRNA In Vitro and In Vivo and Transform Extracellular Vesicles for Their Functional Extensions. *Adv. Sci.* 10, e2206187. <https://doi.org/10.1002/advs.202206187>.
30. Lai, R.C., Arslan, F., Lee, M.M., Sze, N.S.K., Choo, A., Chen, T.S., Salto-Tellez, M., Timmers, L., Lee, C.N., El Oakley, R.M., et al. (2010). Exosome secreted by MSC reduces myocardial ischemia/reperfusion injury. *Stem Cell Res.* 4, 214–222. <https://doi.org/10.1016/j.scr.2009.12.003>.
31. de Abreu, R.C., Fernandes, H., da Costa Martins, P.A., Sahoo, S., Emanueli, C., and Ferreira, L. (2020). Native and bioengineered extracellular vesicles for cardiovascular therapeutics. *Nat. Rev. Cardiol.* 17, 685–697. <https://doi.org/10.1038/s41569-020-0389-5>.
32. Mentkowski, K.I., and Lang, J.K. (2019). Exosomes Engineered to Express a Cardiomyocyte Binding Peptide Demonstrate Improved Cardiac Retention in Vivo. *Sci. Rep.* 9, 10041. <https://doi.org/10.1038/s41598-019-46407-1>.
33. Helfield, B. (2019). A review of phospholipid encapsulated ultrasound contrast agent microbubble physics. *Ultrasound Med. Biol.* 45, 282–300. <https://doi.org/10.1016/j.ultrasmedbio.2018.09.020>.
34. Leighton, T.G. (1994). *The Acoustic Bubble* (Academic Press).
35. Wu, J., and Nyborg, W.L. (2008). Ultrasound, cavitation bubbles and their interaction with cells. *Adv. Drug Deliv. Rev.* 60, 1103–1116. <https://doi.org/10.1016/j.addr.2008.03.009>.
36. Postema, M., van Wamel, A., Lancée, C.T., and de Jong, N. (2004). Ultrasound-induced encapsulated microbubble phenomena. *Ultrasound Med. Biol.* 30, 827–840. <https://doi.org/10.1016/j.ultrasmedbio.2004.02.010>.
37. Apfel, R.E., and Holland, C.K. (1991). Gauging the likelihood of cavitation from short-pulse, low-duty cycle diagnostic ultrasound. *Ultrasound Med. Biol.* 17, 179–185. [https://doi.org/10.1016/0301-5629\(91\)90125-G](https://doi.org/10.1016/0301-5629(91)90125-G).
38. Price, R.J., Skyba, D.M., Kaul, S., and Skalak, T.C. (1998). Delivery of colloidal particles and red blood cells to tissue through microvessel ruptures created by targeted microbubble destruction with ultrasound. *Circulation* 98, 1264–1267. <https://doi.org/10.1161/01.CIR.98.13.1264>.
39. Skyba, D.M., Price, R.J., Linka, A. Z., Skalak, T.C., and Kaul, S. (1998). Direct in vivo visualization of intravascular destruction of microbubbles by ultrasound and its local effects on tissue. *Circulation* 98, 290–293. <https://doi.org/10.1161/01.CIR.98.4.290>.
40. van Wamel, A., Bouakaz, A., Versluis, M., and de Jong, N. (2004). Micromanipulation of endothelial cells: ultrasound-microbubble-cell interaction. *Ultrasound Med. Biol.* 30, 1255–1258. <https://doi.org/10.1016/j.ultrasmedbio.2004.07.015>.
41. Helfield, B., Chen, X., Watkins, S.C., and Villanueva, F.S. (2016). Biophysical insight into mechanisms of sonoporation. *Proc. Natl. Acad. Sci. USA* 113, 9983–9988. <https://doi.org/10.1073/pnas.1606915113>.
42. Park, J., Fan, Z., Kumon, R.E., El-Sayed, M.E.H., and Deng, C.X. (2010). Modulation of intracellular Ca²⁺ concentration in brain microvascular endothelial cells in vitro by acoustic cavitation. *Ultrasound Med. Biol.* 36, 1176–1187. <https://doi.org/10.1016/j.ultrasmedbio.2010.04.006>.
43. Beekers, I., Mastik, F., Beurskens, R., Tang, P.Y., Vegter, M., van der Steen, A.F.W., de Jong, N., Verweij, M.D., and Kooiman, K. (2020). High-Resolution Imaging of Intracellular Calcium Fluctuations Caused by Oscillating Microbubbles. *Ultrasound Med. Biol.* 46, 2017–2029. <https://doi.org/10.1016/j.ultrasmedbio.2020.03.029>.
44. Helfield, B., Chen, X., Watkins, S.C., and Villanueva, F.S. (2020). Transendothelial Perforations and the Sphere of Influence of Single-Site Sonoporation. *Ultrasound Med. Biol.* 46, 1686–1697. <https://doi.org/10.1016/j.ultrasmedbio.2020.02.017>.
45. Belcik, J.T., Davidson, B.P., Xie, A., Wu, M.D., Yadava, M., Qi, Y., Liang, S., Chon, C.R., Ammi, A.Y., Field, J., et al. (2017). Augmentation of Muscle Blood Flow by Ultrasound Cavitation is Mediated by ATP and Purinergic Signaling. *Circulation* 135, 1240–1252.
46. Belcik, J.T., Mott, B.H., Xie, A., Zhao, Y., Kim, S., Lindner, N.J., Ammi, A., Linden, J.M., and Lindner, J.R. (2015). Augmentation of Limb Perfusion and Reversal of Tissue Ischemia Produced by Ultrasound-Mediated Microbubble Cavitation. *Circ. Cardiovasc. Imaging* 8, e002979. <https://doi.org/10.1161/CIRCIMAGING.114.002979>.
47. Chen, H., Kreider, W., Brayman, A.A., Bailey, M.R., and Matula, T.J. (2011). Blood vessel deformations on microsecond time scales by ultrasonic cavitation. *Phys. Rev. Lett.* 106, 034301. <https://doi.org/10.1103/PhysRevLett.106.034301>.
48. Sheikov, N., McDannold, N., Vykhodtseva, N., Jolesz, F., and Hynynen, K. (2004). Cellular mechanisms of the blood-brain barrier opening induced by ultrasound in presence of microbubbles. *Ultrasound Med. Biol.* 30, 979–989. <https://doi.org/10.1016/j.ultrasmedbio.2004.04.010>.
49. Sheikov, N., McDannold, N., Sharma, S., and Hynynen, K. (2008). Effect of focused ultrasound applied with an ultrasound contrast agent on the tight junctional integrity of the brain microvascular endothelium. *Ultrasound Med. Biol.* 34, 1093–1104. <https://doi.org/10.1016/j.ultrasmedbio.2007.12.015>.
50. Meijering, B.D.M., Juffermans, L.J.M., Van Wamel, A., Henning, R.H., Zuhorn, I.S., Emmer, M., Versteilen, A.M.G., Paulus, W.J., Van Gilst, W.H., Kooiman, K., et al. (2009). Ultrasound and microbubble-targeted delivery of macromolecules is regulated by induction of endocytosis and pore formation. *Circ. Res.* 104, 679–687. <https://doi.org/10.1161/CIRCRESAHA.108.183806>.
51. Fekri, F., Delos Santos, R.C., Karshafian, R., and Antonescu, C.N. (2016). Ultrasound microbubble treatment enhances clathrin-mediated endocytosis and fluid-phase uptake through distinct mechanisms. *PLoS One* 11, e0156754. <https://doi.org/10.1371/journal.pone.0156754>.
52. Goertz, D.E. (2015). An overview of the influence of therapeutic ultrasound exposures on the vasculature: High intensity ultrasound and microbubble-mediated bio-effects. *Int. J. Hyperther.* 31, 134–144. <https://doi.org/10.3109/02656736.2015.1009179>.
53. Memari, E., Hui, F., Yusefi, H., and Helfield, B. (2023). Fluid flow influences ultrasound-assisted endothelial membrane permeabilization and calcium flux. *J. Contr. Release* 358, 333–344. <https://doi.org/10.1016/j.jconrel.2023.05.004>.

54. O'Reilly, M.A., Hough, O., and Hynynen, K. (2017). Blood-Brain Barrier closure time after controlled ultrasound-induced opening is independent of opening volume. *J. Ultrasound Med.* 36, 475–483. <https://doi.org/10.7863/ultra.16.02005>.
55. van Rooij, T., Skachkov, I., Beekers, I., Lattwein, K.R., Voorneveld, J.D., Kokhuis, T.J.A., Bera, D., Luan, Y., van der Steen, A.F.W., de Jong, N., and Kooiman, K. (2016). Viability of endothelial cells after ultrasound-mediated sonoporation: Influence of targeting, oscillation, and displacement of microbubbles. *J. Contr. Release* 238, 197–211. <https://doi.org/10.1016/j.jconrel.2016.07.037>.
56. Hu, Y., Wan, J.M.F., and Yu, A.C.H. (2013). Membrane perforation and recovery dynamics in microbubble-mediated sonoporation. *Ultrasound Med. Biol.* 39, 2393–2405. <https://doi.org/10.1016/j.ultrasmedbio.2013.08.003>.
57. Xie, A., Belcik, T., Qi, Y., Morgan, T.K., Champaneri, S. a, Taylor, S., Davidson, B.P., Zhao, Y., Klibanov, A.L., Kuliszewski, M. a, et al. (2012). Ultrasound-mediated vascular gene transfection by cavitation of endothelial-targeted cationic microbubbles. *JACC. Cardiovasc. Imaging* 5, 1253–1262. <https://doi.org/10.1016/j.jcmg.2012.05.017>.
58. Jones, R.M., McMahon, D., and Hynynen, K. (2020). Ultrafast three-dimensional microbubble imaging in vivo predicts tissue damage volume distributions during nonthermal brain ablation. *Theranostics* 10, 7211–7230. <https://doi.org/10.7150/thno.47281>.
59. Chen, Z.Y., Lin, Y., Yang, F., Jiang, L., and Ge, S.P. (2013). Gene therapy for cardiovascular disease mediated by ultrasound and microbubbles. *Cardiovasc. Ultrasound* 11, 11–14. <https://doi.org/10.1186/1476-7120-11-11>.
60. Cho, E.E., Drazic, J., Ganguly, M., Stefanovic, B., and Hynynen, K. (2011). Two-photon fluorescence microscopy study of cerebrovascular dynamics in ultrasound-induced blood – brain barrier opening. *J. Cerebr. Blood Flow Metabol.* 31, 1852–1862. <https://doi.org/10.1038/jcbfm.2011.59>.
61. Yemane, P.T., Åslund, A.K.O., Snipstad, S., Bjørkøy, A., Grendstad, K., Berg, S., Mørch, Y., Torp, S.H., Hansen, R., and Davies, C.d.L. (2019). Effect of Ultrasound on the Vasculature and Extravasation of Nanoscale Particles Imaged in Real Time. *Ultrasound Med. Biol.* 45, 3028–3041. <https://doi.org/10.1016/j.ultrasmedbio.2019.07.683>.
62. Lentacker, I., De Smedt, S.C., and Sanders, N.N. (2009). Drug loaded microbubble design for ultrasound triggered delivery. *Soft Matter* 5, 2161–2170. <https://doi.org/10.1039/b823051j>.
63. Kopechek, J.A., McTiernan, C.F., Chen, X., Zhu, J., Mburu, M., Feroze, R., Whitehurst, D.A., Lavery, L., Cyriac, J., and Villanueva, F.S. (2019). Ultrasound and microbubble-targeted delivery of a microRNA inhibitor to the heart suppresses cardiac hypertrophy and preserves cardiac function. *Theranostics* 9, 7088–7098. <https://doi.org/10.7150/thno.34895>.
64. Meng, Y., Hynynen, K., and Lipsman, N. (2021). Applications of focused ultrasound in the brain: from thermoablation to drug delivery. *Nat. Rev. Neurol.* 17, 7–22. <https://doi.org/10.1038/s41582-020-00418-z>.
65. Kofoed, R.H., and Aubert, I. (2024). Focused ultrasound gene delivery for the treatment of neurological disorders. *Trends Mol. Med.* 30, 263–277. <https://doi.org/10.1016/j.molmed.2023.12.006>.
66. Hynynen, K., McDannold, N., Vykhodtseva, N., and Jolesz, F.A. (2001). Noninvasive MR imaging-guided focal opening of the blood-brain barrier in rabbits. *Radiology* 220, 640–646.
67. McDannold, N., Vykhodtseva, N., and Hynynen, K. (2008). Blood-Brain Barrier Disruption Induced by Focused Ultrasound and Circulating Preformed Microbubbles Appears to Be Characterized by the Mechanical Index. *Ultrasound Med. Biol.* 34, 834–840. <https://doi.org/10.1016/j.ultrasmedbio.2007.10.016>.
68. Wu, S.Y., Sanchez, C.S., Samiotaki, G., Buch, A., Ferrera, V.P., and Konofagou, E.E. (2016). Characterizing Focused-Ultrasound Mediated Drug Delivery to the Heterogeneous Primate Brain in Vivo with Acoustic Monitoring. *Sci. Rep.* 6, 37094. <https://doi.org/10.1038/srep37094>.
69. Arvanitis, C.D., Askoxylakis, V., Guo, Y., Datta, M., Kloepper, J., Ferraro, G.B., Bernabeu, M.O., Fukumura, D., McDannold, N., and Jain, R.K. (2018). Mechanisms of enhanced drug delivery in brain metastases with focused ultrasound-induced blood–tumor barrier disruption. *Proc. Natl. Acad. Sci. USA* 115, E8717–E8726. <https://doi.org/10.1073/pnas.1807105115>.
70. O'Reilly, M.A., and Hynynen, K. (2012). Blood-brain barrier: real-time feedback-controlled focused ultrasound disruption by using an acoustic emissions-based controller. *Radiology* 263, 96–106.
71. Mainprize, T., Lipsman, N., Huang, Y., Meng, Y., Bethune, A., Ironside, S., Heyn, C., Alkins, R., Trudeau, M., Sahgal, A., et al. (2019). Blood-Brain Barrier Opening in Primary Brain Tumors with Non-invasive MR-Guided Focused Ultrasound: A Clinical Safety and Feasibility Study. *Sci. Rep.* 9, 321. <https://doi.org/10.1038/s41598-018-36340-0>.
72. Carpentier, A., Stupp, R., Sonabend, A.M., Dufour, H., Chinot, O., Mathon, B., Ducray, F., Guyotat, J., Baize, N., Menei, P., et al. (2024). Repeated blood–brain barrier opening with a nine-emitter implantable ultrasound device in combination with carboplatin in recurrent glioblastoma: a phase I/II clinical trial. *Nat. Commun.* 15, 1650. <https://doi.org/10.1038/s41467-024-45818-7>.
73. Meng, Y., Reilly, R.M., Pezo, R.C., Trudeau, M., Sahgal, A., Singnurkar, A., Perry, J., Myrehaug, S., Pople, C.B., Davidson, B., et al. (2021). MR-guided focused ultrasound enhances delivery of trastuzumab to Her2-positive brain metastases. *Sci. Transl. Med.* 13, eabj4011. <https://doi.org/10.1126/scitranslmed.abj4011>.
74. Memari, E., Khan, D., Alkins, R., and Helfield, B. (2024). Focused ultrasound-assisted delivery of immunomodulating agents in brain cancer. *J. Contr. Release* 367, 283–299. <https://doi.org/10.1016/j.jconrel.2024.01.034>.
75. Jones, R.M., and Hynynen, K. (2019). Advances in acoustic monitoring and control of focused ultrasound-mediated increases in blood-brain barrier permeability. *Br. J. Radiol.* 92, 20180601–20180613. <https://doi.org/10.1259/bjr.20180601>.
76. Lee, H., Guo, Y., Ross, J.L., Schoen, S., Degertekin, F.L., and Arvanitis, C. (2022). Spatially targeted brain cancer immunotherapy with closed-loop controlled focused ultrasound and immune checkpoint blockade. *Sci. Adv.* 8, eadd2288. <https://doi.org/10.1126/sciadv.add2288>.
77. Anastasiadis, P., Gandhi, D., Guo, Y., Ahmed, A.K., Bentzen, S.M., Arvanitis, C., and Woodworth, G.F. (2021). Localized blood-brain barrier opening in infiltrating gliomas with MRI-guided acoustic emissions-controlled focused ultrasound. *Proc. Natl. Acad. Sci. USA* 118, e2103280118. <https://doi.org/10.1073/pnas.2103280118>.
78. Hughes, A., Khan, D.S., and Alkins, R. (2023). Current and Emerging Systems for Focused Ultrasound-Mediated Blood–Brain Barrier Opening. *Ultrasound Med. Biol.* 49, 1479–1490. <https://doi.org/10.1016/j.ultrasmedbio.2023.02.017>.
79. Sonoda, S., Tachibana, K., Uchino, E., Okubo, A., Yamamoto, M., Sakoda, K., Hisatomi, T., Sonoda, K.H., Negishi, Y., Izumi, Y., et al. (2006). Gene transfer to corneal epithelium and keratocytes mediated by ultrasound with microbubbles. *Invest. Ophthalmol. Vis. Sci.* 47, 558–564. <https://doi.org/10.1167/iovs.05-0889>.
80. Sakakima, Y., Hayashi, S., Yagi, Y., Hayakawa, A., Tachibana, K., and Nakao, A. (2005). Gene therapy for hepatocellular carcinoma using sonoporation enhanced by contrast agents. *Cancer Gene Ther.* 12, 884–889. <https://doi.org/10.1038/sj.cgt.7700850>.
81. Chen, S., Ding, J.-H., Bekerredjian, R., Yang, B.-Z., Shohet, R.V., Johnston, S.A., Hohmeier, H.E., Newgard, C.B., and Grayburn, P.A. (2006). Efficient Gene Delivery to Pancreatic Islets with Ultrasonic Microbubble Destruction Technology. *Ultrasound-targeted microbubble destruction can repeatedly direct highly specific plasmid expression to the heart. Circulation* 108, 1022–1026.
82. Wolfram, J.A., and Donahue, J.K. (2013). Gene Therapy to Treat Cardiovascular Disease. *J. Am. Heart Assoc.* 2, e000119. <https://doi.org/10.1161/JAHA.113.000119>.
83. Shohet, R.V., Chen, S., Zhou, Y.-T., Wang, Z., Meidell, R.S., Unger, R.H., and Grayburn, P.a. (2000). Echocardiographic Destruction of Albumin Microbubbles Directs Gene Delivery to the Myocardium. *Circulation* 101, 2554–2556. <https://doi.org/10.1161/01.CIR.101.22.2554>.
84. Bekerredjian, R., Chen, S., Frenkel, P.A., Grayburn, P.A., and Shohet, R.V. (2003). Ultrasound-targeted microbubble destruction can repeatedly direct highly specific plasmid expression to the heart. *Circulation* 108, 1022–1026.
85. Kondo, I., Ohmori, K., Oshita, A., Takeuchi, H., Fuke, S., Shinomiya, K., Noma, T., Namba, T., and Kohno, M. (2004). Treatment of acute myocardial infarction by hepatocyte growth factor gene transfer: The first demonstration of myocardial transfer of a “functional” gene using ultrasonic microbubble destruction. *J. Am. Coll. Cardiol.* 44, 644–653. <https://doi.org/10.1016/j.jacc.2004.04.042>.
86. Ueda, H., Sawa, Y., Matsumoto, K., Kitagawa-Sakakida, S., Kawahira, Y., Nakamura, T., Kaneda, Y., and Matsuda, H. (1999). Gene transfection of hepatocyte growth factor attenuates reperfusion injury in the heart. *Ann. Thorac. Surg.* 67, 1726–1731. [https://doi.org/10.1016/S0003-4975\(99\)00279-9](https://doi.org/10.1016/S0003-4975(99)00279-9).

87. Wang, W., Tayier, B., Guan, L., Yan, F., and Mu, Y. (2022). Pre-transplantation of bone marrow mesenchymal stem cells amplifies the therapeutic effect of ultrasound-targeted microbubble destruction-mediated localized combined gene therapy in post-myocardial infarction heart failure rats. *Ultrasound Med. Biol.* 48, 830–845. <https://doi.org/10.1016/j.ultrasmedbio.2022.01.004>.
88. Erikson, J.M., Freeman, G.L., and Chandrasekar, B. (2003). Ultrasound-targeted antisense oligonucleotide attenuates ischemia/reperfusion-induced myocardial tumor necrosis factor- α . *J. Mol. Cell. Cardiol.* 35, 119–130. [https://doi.org/10.1016/S0022-2828\(02\)00289-4](https://doi.org/10.1016/S0022-2828(02)00289-4).
89. Mofid, A., Newman, N.S., Lee, P.J.H., Abbasi, C., Matkar, P.N., Rudenko, D., Kuliszewski, M.A., Chen, H.H., Afrasiabi, K., Tsoporis, J.N., et al. (2017). Cardiac overexpression of S100A6 attenuates cardiomyocyte apoptosis and reduces infarct size after myocardial ischemia-reperfusion. *J. Am. Heart Assoc.* 6, e004738. <https://doi.org/10.1161/JAHA.116.004738>.
90. Ciarambino, T., Menna, G., Sansone, G., and Giordano, M. (2021). Cardiomyopathies : An Overview. *Int. J. Mol. Sci.* 22, 7722–7725.
91. Lee, P.J.H., Rudenko, D., Kuliszewski, M.A., Liao, C., Kabir, M.G., Connelly, K.A., and Leong-poi, H. (2014). Survivin gene therapy attenuates left ventricular systolic dysfunction in doxorubicin cardiomyopathy by reducing apoptosis and fibrosis. *Cardiovasc. Res.* 101, 423–433. <https://doi.org/10.1093/cvr/cvu001>.
92. Qin, X., Cai, P., Liu, C., Chen, K., Jiang, X., Chen, W., Li, J., Jiao, X., Guo, E., Yu, Y., et al. (2023). Cardioprotective effect of ultrasound-targeted destruction of Sirt3-loaded cationic microbubbles in a large animal model of pathological cardiac hypertrophy. *Acta Biomater.* 164, 604–625. <https://doi.org/10.1016/j.actbio.2023.04.020>.
93. Sun, L., Huang, C.W., Wu, J., Chen, K.J., Li, S.H., Weisel, R.D., Rakowski, H., Sung, H.W., and Li, R.K. (2013). The use of cationic microbubbles to improve ultrasound-targeted gene delivery to the ischemic myocardium. *Biomaterials* 34, 2107–2116. <https://doi.org/10.1016/j.biomaterials.2012.11.041>.
94. Kooiman, K., Vos, H.J., Versluis, M., and de Jong, N. (2014). Acoustic behavior of microbubbles and implications for drug delivery. *Adv. Drug Deliv. Rev.* 72, 28–48. <https://doi.org/10.1016/j.addr.2014.03.003>.
95. Fujii, H., Li, S.H., Wu, J., Miyagi, Y., Yau, T.M., Rakowski, H., Egashira, K., Guo, J., Weisel, R.D., and Li, R.K. (2011). Repeated and targeted transfer of angiogenic plasmids into the infarcted rat heart via ultrasound targeted microbubble destruction enhances cardiac repair. *Eur. Heart J.* 32, 2075–2084. <https://doi.org/10.1093/eurheartj/ehq475>.
96. Kaufmann, B. a, Sanders, J.M., Davis, C., Xie, A., Aldred, P., Sarembock, I.J., and Lindner, J.R. (2007). Molecular imaging of inflammation in atherosclerosis with targeted ultrasound detection of vascular cell adhesion molecule-1. *Circulation* 116, 276–284. <https://doi.org/10.1161/CIRCULATIONAHA.106.684738>.
97. Hamilton, A.J., Huang, S.L., Warnick, D., Rabbat, M., Kane, B., Nagaraj, A., Klegerman, M., and McPherson, D.D. (2004). Intravascular Ultrasound Molecular Imaging of Atheroma Components In Vivo. *J. Am. Coll. Cardiol.* 43, 453–460. <https://doi.org/10.1016/j.jacc.2003.07.048>.
98. Villanueva, F.S., Jankowski, R.J., Klibanov, S., Pina, M.L., Alber, S.M., Watkins, S.C., Brandenburger, G.H., and Wagner, W.R. (1998). Microbubbles targeted to intercellular adhesion molecule-1 bind to activated coronary artery endothelial cells. *Circulation* 98, 1–5.
99. Lindner, J.R., Song, J., Christiansen, J., Klibanov, A. L., Xu, F., and Ley, K. (2001). Ultrasound assessment of inflammation and renal tissue injury with microbubbles targeted to P-selectin. *Circulation* 104, 2107–2112.
100. Davidson, B.P., Kaufmann, B.A., Belcik, J.T., Xie, A., Qi, Y., and Lindner, J.R. (2012). Detection of antecedent myocardial ischemia with multiselectin molecular imaging. *J. Am. Coll. Cardiol.* 60, 1690–1697. <https://doi.org/10.1016/j.jacc.2012.07.027>.
101. Pochon, S., Tardy, I., Bussat, P., Bettinger, T., Brochot, J., von Wronski, M., Passantino, L., and Schneider, M. (2010). BR55: a lipopeptide-based VEGFR2-targeted ultrasound contrast agent for molecular imaging of angiogenesis. *Invest. Radiol.* 45, 89–95. <https://doi.org/10.1097/RLI.0b013e3181c5927c>.
102. Mott, B., Packwood, W., Xie, A., Belcik, J.T., Taylor, R.P., Zhao, Y., Davidson, B.P., and Lindner, J.R. (2016). Echocardiographic Ischemic Memory Imaging Through Complement-Mediated Vascular Adhesion of Phosphatidylserine-Containing Microbubbles. *JACC. Cardiovasc. Imaging* 9, 937–946. <https://doi.org/10.1016/j.jcmg.2015.11.031>.
103. Zhou, Q., Deng, Q., Hu, B.O., Wang, Y.J., Chen, J.L., Cui, J.J., Cao, S., and Song, H.N. (2017). Ultrasound combined with targeted cationic microbubble-mediated angiogenesis gene transfection improves ischemic heart function. *Exp. Ther. Med.* 13, 2293–2303. <https://doi.org/10.3892/etm.2017.4270>.
104. Takeuchi, H., Ohmori, K., Kondo, I., Oshita, A., Shinomiya, K., Yu, Y., Takagi, Y., Mizushige, K., Kangawa, K., and Kohno, M. (2003). Potentiation of C-type natriuretic peptide with ultrasound and microbubbles to prevent neointimal formation after vascular injury in rats. *Cardiovasc. Res.* 58, 231–238. [https://doi.org/10.1016/S0008-6363\(02\)00833-7](https://doi.org/10.1016/S0008-6363(02)00833-7).
105. Kobulnik, J., Kuliszewski, M.A., Stewart, D.J., Lindner, J.R., and Leong-Poi, H. (2009). Comparison of gene delivery techniques for therapeutic angiogenesis ultrasound-mediated destruction of carrier microbubbles versus direct intramuscular injection. *J. Am. Coll. Cardiol.* 54, 1735–1742. <https://doi.org/10.1016/j.jacc.2009.07.023>.
106. Chen, H., Kuliszewski, M.A., Rudenko, D., and Leong-Poi, H. (2017). Preclinical Evaluation of Proangiogenic Gene Therapy by Ultrasound Targeted Microbubble Destruction of Vascular Endothelial Growth Factor Minicircle DNA in a Model of Severe Peripheral Arterial Disease in Watanabe Heritable Hyperlipidemic Rabbits (abstrac. *Circulation* 136, A19897.
107. Smith, A.H., Kuliszewski, M.A., Liao, C., Rudenko, D., Stewart, D.J., and Leong-Poi, H. (2012). Sustained improvement in perfusion and flow reserve after temporally separated delivery of vascular endothelial growth factor and angiopoietin-1 plasmid deoxyribonucleic acid. *J. Am. Coll. Cardiol.* 59, 1320–1328. <https://doi.org/10.1016/j.jacc.2011.12.025>.
108. Kuliszewski, M.A., Kobulnik, J., Lindner, J.R., Stewart, D.J., and Leong-Poi, H. (2011). Vascular gene transfer of SDF-1 promotes endothelial progenitor cell engraftment and enhances angiogenesis in ischemic muscle. *Mol. Ther.* 19, 895–902. <https://doi.org/10.1038/mt.2011.18>.
109. Cao, W.J., Rosenblat, J.D., Roth, N.C., Kuliszewski, M.A., Matkar, P.N., Rudenko, D., Liao, C., Lee, P.J.H., and Leong-Poi, H. (2015). Therapeutic Angiogenesis by Ultrasound-Mediated MicroRNA-126-3p Delivery. *Arterioscler. Thromb. Vasc. Biol.* 35, 2401–2411. <https://doi.org/10.1161/ATVBAHA.115.306506>.
110. Song, J., Qi, M., Kaul, S., and Price, R.J. (2002). Stimulation of arteriogenesis in skeletal muscle by microbubble destruction with ultrasound. *Circulation* 106, 1550–1555. <https://doi.org/10.1161/01.CIR.0000028810.33423.95>.
111. Song, J., Cottler, P.S., Klibanov, A.L., Kaul, S., and Price, R.J. (2004). Microvascular remodeling and accelerated hyperemia blood flow restoration in arterially occluded skeletal muscle exposed to ultrasonic microbubble destruction. *Am. J. Physiol. Heart Circ. Physiol.* 287, 2754–2761. <https://doi.org/10.1152/ajpheart.00144.2004>.
112. Yoshida, J., Ohmori, K., Takeuchi, H., Shinomiya, K., Namba, T., Kondo, I., Kiyomoto, H., and Kohno, M. (2005). Treatment of ischemic limbs based on local recruitment of vascular endothelial growth factor-producing inflammatory cells with ultrasonic microbubble destruction. *J. Am. Coll. Cardiol.* 46, 899–905. <https://doi.org/10.1016/j.jacc.2005.05.052>.
113. Zhang, X., Tian, X., Li, P., Zhu, H., Zhou, N., Fang, Z., Yang, Y., Jing, Y., and Yuan, J. (2021). Ultrasound-targeted microbubble destruction promotes myocardial angiogenesis and functional improvements in rat model of diabetic cardiomyopathy. *BMC Cardiovasc. Disord.* 21, 21–29. <https://doi.org/10.1186/s12872-020-01815-4>.
114. Zhou, N.Q., Song, Y.T., Liu, W.Z., Yue, R.Z., Tian, X.Q., Yang, S.C., Yin, Y.L., and Li, P. (2023). Diagnostic ultrasound-mediated microbubble cavitation dose-dependently improves diabetic cardiomyopathy through angiogenesis. *Cell Biol. Int.* 47, 178–187. <https://doi.org/10.1002/cbin.11918>.
115. Anderson, C.D., Arthur, J.A., Zhang, Y., Bharucha, N., Karakikes, I., and Shohet, R.V. (2023). Non-viral in vivo cytidine base editing in hepatocytes using focused ultrasound targeted microbubbles. *Mol. Ther. Nucleic Acids* 33, 733–737. <https://doi.org/10.1016/j.omtn.2023.07.032>.
116. Paranjape, A.N., D’Aiuto, L., Zheng, W., Chen, X., and Villanueva, F.S. (2024). A multicellular brain spheroid model for studying the mechanisms and bioeffects of ultrasound-enhanced drug penetration beyond the blood–brain barrier. *Sci. Rep.* 14, 1909. <https://doi.org/10.1038/s41598-023-50203-3>.
117. Wu, J., Xie, F., Kumar, T., Liu, J., Lof, J., Shi, W., Everbach, E.C., and Porter, T.R. (2014). Improved sonothrombolysis from a modified diagnostic transducer delivering impulses containing a longer pulse duration. *Ultrasound Med. Biol.* 40, 1545–1553. <https://doi.org/10.1016/j.ultrasmedbio.2014.01.015>.

118. Cao, S., Deng, Q., Wang, Y., Zhou, Y., and Zhou, Q. (2021). Ultrasound-targeted microbubble destruction-mediated Ang1 gene transfection improves left ventricular structural and sympathetic nerve remodeling in canines with myocardial infarction. *Ann. Transl. Med.* 9, 221. <https://doi.org/10.21037/atm-20-839>.
119. Suzuki, J.I., Ogawa, M., Takayama, K., Taniyama, Y., Morishita, R., Hirata, Y., Nagai, R., and Isoe, M. (2010). Ultrasound-Microbubble-Mediated Intercellular Adhesion Molecule-1 Small Interfering Ribonucleic Acid Transfection Attenuates Neointimal Formation After Arterial Injury in Mice. *J. Am. Coll. Cardiol.* 55, 904–913. <https://doi.org/10.1016/j.jacc.2009.09.054>.
120. Wang, Z., Jiang, S., Li, S., Yu, W., Chen, J., Yu, D., Zhao, C., Li, Y., Kang, K., Wang, R., et al. (2020). Targeted galectin-7 inhibition with ultrasound microbubble targeted gene therapy as a sole therapy to prevent acute rejection following heart transplantation in a Rodent model. *Biomaterials* 263, 120366. <https://doi.org/10.1016/j.biomaterials.2020.120366>.
121. Sun, W., Zhao, P., Zhou, Y., Xing, C., Zhao, L., Li, Z., and Yuan, L. (2020). Ultrasound targeted microbubble destruction assisted exosomal delivery of miR-21 protects the heart from chemotherapy associated cardiotoxicity. *Biochem. Biophys. Res. Commun.* 532, 60–67. <https://doi.org/10.1016/j.bbrc.2020.05.044>.
122. Yi, L., Chen, Y., Jin, Q., Deng, C., Wu, Y., Li, H., Liu, T., Li, Y., Yang, Y., Wang, J., et al. (2020). Antagomir-155 Attenuates Acute Cardiac Rejection Using Ultrasound Targeted Microbubbles Destruction. *Adv. Healthcare Mater.* 9, 20001899–e2000210. <https://doi.org/10.1002/adhm.202000189>.
123. Chen, S., Chen, J., Huang, P., Meng, X.L., Clayton, S., Shen, J.S., and Grayburn, P.A. (2015). Myocardial regeneration in adriamycin cardiomyopathy by nuclear expression of GLP1 using ultrasound targeted microbubble destruction. *Biochem. Biophys. Res. Commun.* 458, 823–829. <https://doi.org/10.1016/j.bbrc.2015.02.038>.
124. Chen, S., Chen, J., Meng, X.L., Shen, J.S., Huang, J., Huang, P., Pu, Z., McNeill, N.H., and Grayburn, P.A. (2016). ANGPTL8 reverses established adriamycin cardiomyopathy by stimulating adult cardiac progenitor cells. *Oncotarget* 7, 80391–80403. <https://doi.org/10.18632/oncotarget.13061>.
125. Giacca, M., and Zacchigna, S. (2012). VEGF gene therapy: Therapeutic angiogenesis in the clinic and beyond. *Gene Ther.* 19, 622–629. <https://doi.org/10.1038/gt.2012.17>.
126. Isner, J.M. (2002). Myocardial gene therapy. *Nature* 415, 234–239. <https://doi.org/10.1038/415234a>.
127. Del Monte, F., Williams, E., Lebeche, D., Schmidt, U., Rosenzweig, A., Gwathmey, J.K., Lewandowski, E.D., and Hajjar, R.J. (2001). Improvement in survival and cardiac metabolism after gene transfer of sarcoplasmic reticulum Ca²⁺-ATPase in a rat model of heart failure. *Circulation* 104, 1424–1429. <https://doi.org/10.1161/hc3601.095574>.
128. Lai, N.C., Roth, D.M., Gao, M.H., Tang, T., Dalton, N., Lai, Y.Y., Spellman, M., Clopton, P., and Hammond, H.K. (2004). Intracoronary adenovirus encoding adenylyl cyclase VI increases left ventricular function in heart failure. *Circulation* 110, 330–336. <https://doi.org/10.1161/01.CIR.0000136033.21777.AD>.
129. Kato, K., Yin, H., Agata, J., Yoshida, H., Chao, L., and Chao, J. (2003). Adrenomedullin gene delivery attenuates myocardial infarction and apoptosis after ischemia and reperfusion. *Am. J. Physiol. Heart Circ. Physiol.* 285, 1506–1514. <https://doi.org/10.1152/ajpheart.00270.2003>.
130. Chatterjee, S., Stewart, A.S., Bish, L.T., Jayasankar, V., Kim, E.M., Pirolli, T., Burdick, J., Woo, Y.J., Gardner, T.J., and Sweeney, H.L. (2002). Viral gene transfer of the antiapoptotic factor Bcl-2 protects against chronic posts ischemic heart failure. *Circulation* 106, 212–217. <https://doi.org/10.1161/01.cir.0000032907.33237.55>.
131. He, Z., Li, H., Zuo, S., Pasha, Z., Wang, Y., Yang, Y., Jiang, W., Ashraf, M., and Xu, M. (2011). Transduction of Wnt11 promotes mesenchymal stem cell transdifferentiation into cardiac phenotypes. *Stem Cell. Dev.* 20, 1771–1778. <https://doi.org/10.1089/scd.2010.0380>.
132. Pepe, M., Mamdani, M., Zentilin, L., Csiszar, A., Qanun, K., Zacchigna, S., Ungvari, Z., Puligadda, U., Moimas, S., Xu, X., et al. (2010). Intramyocardial VEGF-B167 gene delivery delays the progression towards congestive failure in dogs with pacing-induced dilated cardiomyopathy. *Circ. Res.* 106, 1893–1903. <https://doi.org/10.1161/CIRCRESAHA.110.220855>.
133. Pachori, A.S., Melo, L.G., Zhang, L., Solomon, S.D., and Dzau, V.J. (2006). Chronic recurrent myocardial ischemic injury is significantly attenuated by pre-emptive adeno-associated virus heme oxygenase-1 gene delivery. *J. Am. Coll. Cardiol.* 47, 635–643. <https://doi.org/10.1016/j.jacc.2005.09.038>.
134. Sundararaman, S., Miller, T.J., Pastore, J.M., Kiedrowski, M., Aras, R., and Penn, M.S. (2011). Plasmid-based transient human stromal cell-derived factor-1 gene transfer improves cardiac function in chronic heart failure. *Gene Ther.* 18, 867–873. <https://doi.org/10.1038/gt.2011.18>.
135. Askari, A.T., Unzek, S., Popovic, Z.B., Goldman, C.K., Forudi, F., Kiedrowski, M., Rovner, A., Ellis, S.G., Thomas, J.D., Dicorleto, P.E., et al. (2003). Effect of stromal-cell-derived factor 1 on stem-cell homing and tissue regeneration in ischaemic cardiomyopathy. *Lancet* 362, 697–703.
136. Sun, Z., Xie, Y., Lee, R.J., Chen, Y., Jin, Q., Lv, Q., Wang, J., Yang, Y., Li, Y., Cai, Y., et al. (2020). Myocardium-targeted transplantation of PHD2 shRNA-modified bone mesenchymal stem cells through ultrasound-targeted microbubble destruction protects the heart from acute myocardial infarction. *Theranostics* 10, 4967–4982. <https://doi.org/10.7150/thno.43233>.
137. Zhang, L., Sun, Z., Ren, P., You, M., Zhang, J., Fang, L., Wang, J., Chen, Y., Yan, F., Zheng, H., and Xie, M. (2017). Localized delivery of shRNA against PHD2 protects the heart from acute myocardial infarction through ultrasound-targeted cationic microbubble destruction. *Theranostics* 7, 51–66. <https://doi.org/10.7150/thno.16074>.
138. Deng, Q., Hu, B., Cao, S., Song, H.N., Chen, J.L., and Zhou, Q. (2015). Improving the efficacy of therapeutic angiogenesis by UTMD-mediated Ang-1 gene delivery to the infarcted myocardium. *Int. J. Mol. Med.* 36, 335–344. <https://doi.org/10.3892/ijmm.2015.2226>.
139. Liu, Y., Li, L., Su, Q., Liu, T., Ma, Z., and Yang, H. (2015). Ultrasound-targeted microbubble destruction enhances gene expression of microRNA-21 in swine heart via intracoronary delivery. *Echocardiography* 32, 1407–1416. <https://doi.org/10.1111/echo.12876>.
140. Li, L., Wu, S., Liu, Z., Zhuo, Z., Tan, K., Xia, H., Zhuo, L., Deng, X., Gao, Y., and Xu, Y. (2015). Ultrasound-Targeted Microbubble Destruction Improves the Migration and Homing of Mesenchymal Stem Cells after Myocardial Infarction by Upregulating SDF-1/CXCR4: A Pilot Study. *Stem Cell. Int.* 2015, 691310. <https://doi.org/10.1155/2015/691310>.
141. Zhou, Z., Zhang, P., Ren, J., Ran, H., Zheng, Y., Li, P., Zhang, Q., Zhang, M., and Wang, Z. (2013). Synergistic effects of ultrasound-targeted microbubble destruction and TAT peptide on gene transfection: An experimental study in vitro and in vivo. *J. Contr. Release* 170, 437–444. <https://doi.org/10.1016/j.jconrel.2013.06.005>.
142. Ling, Z.Y., Shu, S.Y., Zhong, S.G., Luo, J., Su, L., Liu, Z.Z., Lan, X.B., Yuan, G.B., Zheng, Y.Y., Ran, H.T., et al. (2013). Ultrasound targeted microbubble destruction promotes angiogenesis and heart function by inducing myocardial microenvironment change. *Ultrasound Med. Biol.* 39, 2001–2010. <https://doi.org/10.1016/j.ultrasmedbio.2013.06.003>.
143. Yuan, Q.Y., Huang, J., Chu, B.C., Li, X.J., Li, X.S., and Si, L.Y. (2012). A targeted high-efficiency angiogenesis strategy as therapy for myocardial infarction. *Life Sci.* 90, 695–702. <https://doi.org/10.1016/j.lfs.2012.03.003>.
144. Zhong, S., Shu, S., Wang, Z., Luo, J., Zhong, W., Ran, H., Zheng, Y., Yin, Y., and Ling, Z. (2012). Enhanced homing of mesenchymal stem cells to the ischemic myocardium by ultrasound-targeted microbubble destruction. *Ultrasonics* 52, 281–286. <https://doi.org/10.1016/j.ultras.2011.08.013>.
145. Xu, Y.L., Gao, Y.H., Liu, Z., Tan, K.B., Hua, X., Fang, Z.Q., Wang, Y.L., Wang, Y.J., Xia, H.M., and Zhuo, Z.X. (2010). Myocardium-targeted transplantation of mesenchymal stem cells by diagnostic ultrasound-mediated microbubble destruction improves cardiac function in myocardial infarction of New Zealand rabbits. *Int. J. Cardiol.* 138, 182–195. <https://doi.org/10.1016/j.ijcard.2009.03.071>.
146. Fujii, H., Sun, Z., Li, S.-H., Wu, J., Fazel, S., Weisel, R.D., Rakowski, H., Lindner, J., and Li, R.-K. (2009). Ultrasound-Targeted Gene Delivery Induces Angiogenesis After a Myocardial Infarction in Mice. *JACC. Cardiovasc. Imaging* 2, 869–879. <https://doi.org/10.1016/j.jcmg.2009.04.008>.
147. Erikson, J.M., Valente, A.J., Mummidi, S., Kandikattu, H.K., Demarco, V.G., Bender, S.B., Fay, W.P., Siebenlist, U., and Chandrasekar, B. (2017). Targeting TRAF3IP2 by genetic and interventional approaches inhibits ischemia/reperfusion-induced myocardial injury and adverse remodeling. *J. Biol. Chem.* 292, 2345–2358. <https://doi.org/10.1074/jbc.M116.764522>.

148. Du, G.Q., Shao, Z.B., Wu, J., Yin, W.J., Li, S.H., Wu, J., Weisel, R.D., Tian, J.W., and Li, R.K. (2017). Targeted myocardial delivery of GDF11 gene rejuvenates the aged mouse heart and enhances myocardial regeneration after ischemia–reperfusion injury. *Basic Res. Cardiol.* *112*, 7–14. <https://doi.org/10.1007/s00395-016-0593-y>.
149. Kwekkeboom, R.F.J., Sluijter, J.P.G., Van Middelaar, B.J., Metz, C.H., Brans, M.A., Kamp, O., Paulus, W.J., and Musters, R.J.P. (2016). Increased local delivery of anti-gomir therapeutics to the rodent myocardium using ultrasound and microbubbles. *J. Contr. Release* *222*, 18–31. <https://doi.org/10.1016/j.jconrel.2015.11.020>.
150. Yan, P., Chen, K.J., Wu, J., Sun, L., Sung, H.W., Weisel, R.D., Xie, J., and Li, R.K. (2014). The use of MMP2 antibody-conjugated cationic microbubble to target the ischemic myocardium, enhance Timp3 gene transfection and improve cardiac function. *Biomaterials* *35*, 1063–1073. <https://doi.org/10.1016/j.biomaterials.2013.10.043>.
151. Gao, J., Liu, J., Meng, Z., Li, Y., Hong, Y., Wang, L., He, L., Hu, B., Zheng, Y., Li, T., et al. (2021). Ultrasound-assisted C3F8-filled PLGA nanobubbles for enhanced FGF21 delivery and improved prophylactic treatment of diabetic cardiomyopathy. *Acta Biomater.* *130*, 395–408. <https://doi.org/10.1016/j.actbio.2021.06.015>.
152. Zheng, L., Shen, C.L., Li, J.M., Ma, Y.L., Yan, N., Tian, X.Q., and Zhao, Y.Z. (2019). Assessment of the preventive effect against diabetic cardiomyopathy of FGF1-loaded nanoliposomes combined with microbubble cavitation by ultrasound. *Front. Pharmacol.* *10*, 1535–1612. <https://doi.org/10.3389/fphar.2019.01535>.
153. Tian, X.Q., Ni, X.W., Xu, H.L., Zheng, L., ZhuGe, D.L., Chen, B., Lu, C.T., Yuan, J.J., and Zhao, Y.Z. (2017). Prevention of doxorubicin-induced cardiomyopathy using targeted MaFGF mediated by nanoparticles combined with ultrasound-targeted MB destruction. *Int. J. Nanomed.* *12*, 7103–7119. <https://doi.org/10.2147/IJN.S145799>.
154. Feroze, R.A., Kopechek, J., Zhu, J., Chen, X., and Villanueva, F.S. (2023). Ultrasound-Induced Microbubble Cavitation for Targeted Delivery of MiR-29b Mimic to Treat Cardiac Fibrosis. *Ultrasound Med. Biol.* *49*, 2573–2580. <https://doi.org/10.1016/j.ultrasmedbio.2023.08.025>.
155. Li, W., Jin, Q., Zhang, L., He, S., Song, Y., Xu, L., Deng, C., Wang, L., Qin, X., and Xie, M. (2023). Ultrasonic Microbubble Cavitation Deliver Gal-3 shRNA to Inhibit Myocardial Fibrosis after Myocardial Infarction. *Pharmaceutics* *15*, 729–813.
156. Su, Q., Li, L., Liu, Y., Zhou, Y., Wang, J., and Wen, W. (2015). Ultrasound-targeted microbubble destruction-mediated microRNA-21 transfection regulated PDCD4/NF- κ B/TNF- α pathway to prevent coronary microembolization-induced cardiac dysfunction. *Gene Ther.* *22*, 1000–1006. <https://doi.org/10.1038/gt.2015.59>.